Molecular Cell

Article

A peroxiredoxin-P38 MAPK scaffold increases MAPK activity by MAP3K-independent mechanisms

Graphical abstract

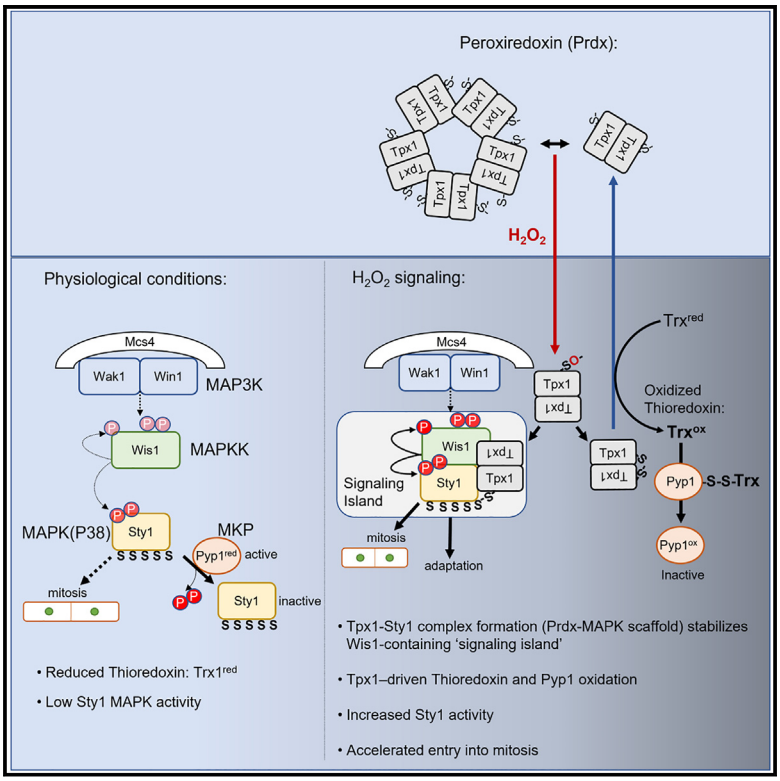

Highlights

- P38-Prdx complexes increase P38 (Sty1/MAPK14) phosphorylation in yeast and human cells
- The *S. pombe* Prdx Tpx1 promotes thioredoxin-dependent oxidation of a MAPK phosphatase
- Sty1-Tpx1 complex activity is increased by phosphatase and MAP3K-independent mechanisms
- Sty1-Tpx1 complexes form a scaffold supporting non-canonical activation of the Wis1 MAPKK

Authors

Min Cao, Alison M. Day, Martin Galler, ..., Brian A. Morgan, Patrick A. Eyers, Elizabeth A. Veal

Correspondence

e.a.veal@ncl.ac.uk

In brief

Phosphorylation activates P38 MAPK in response to many stimuli. Cao et al. reveal two mechanisms by which a peroxiredoxin transmits H_2O_2 signals to P38: (1) forming a Prdx-P38 complex that provides a scaffold for non-canonical activation of P38 MAPKK and (2) alleviating inhibition by a redox-sensitive P38 phosphatase.

Cao et al., 2023, Molecular Cell *83*, 3140–3154
September 7, 2023 Crown Copyright © 2023 Published by Elsevier Inc.
https://doi.org/10.1016/j.molcel.2023.07.018

CellPress

CellPress
OPEN ACCESS

Molecular Cell

Article

A peroxiredoxin-P38 MAPK scaffold increases MAPK activity by MAP3K-independent mechanisms

Min Cao,[1,4] Alison M. Day,[1,4] Martin Galler,[1,4] Heather R. Latimer,[1] Dominic P. Byrne,[2] Thomas W. Foy,[1] Emilia Dwyer,[1] Elise Bennett,[1] Jeremy Palmer,[3] Brian A. Morgan,[1] Patrick A. Eyers,[2] and Elizabeth A. Veal[1,5,*]

[1]Newcastle University Biosciences Institute, Faculty of Medical Sciences, Newcastle University, Framlington Place, Newcastle upon Tyne NE2 4HH, UK

[2]Department of Biochemistry and Systems Biology, Institute of Systems, Molecular and Integrative Biology, University of Liverpool, Liverpool L69 7ZB, UK

[3]Newcastle University Translational and Clinical Research Institute, Faculty of Medical Sciences, Newcastle University, Framlington Place, Newcastle upon Tyne NE2 4HH, UK

[4]These authors contributed equally

[5]Lead contact

*Correspondence: e.a.veal@ncl.ac.uk

https://doi.org/10.1016/j.molcel.2023.07.018

SUMMARY

Peroxiredoxins (Prdxs) utilize reversibly oxidized cysteine residues to reduce peroxides and promote H_2O_2 signal transduction, including H_2O_2-induced activation of P38 MAPK. Prdxs form H_2O_2-induced disulfide complexes with many proteins, including multiple kinases involved in P38 MAPK signaling. Here, we show that a genetically encoded fusion between a Prdx and P38 MAPK is sufficient to hyperactivate the kinase in yeast and human cells by a mechanism that does not require the H_2O_2-sensing cysteine of the Prdx. We demonstrate that a P38-Prdx fusion protein compensates for loss of the yeast scaffold protein Mcs4 and MAP3K activity, driving yeast into mitosis. Based on our findings, we propose that the H_2O_2-induced formation of Prdx-MAPK disulfide complexes provides an alternative scaffold and signaling platform for MAPKK-MAPK signaling. The demonstration that formation of a complex with a Prdx is sufficient to modify the activity of a kinase has broad implications for peroxide-based signal transduction in eukaryotes.

INTRODUCTION

Cells have evolved an array of sensing mechanisms to protect themselves against damaging reactive oxygen species. These include redox-active peroxiredoxins (Prdxs), which form a key part of the cellular defense against peroxides and play central roles in aging and cancer.[1] The thioredoxin peroxidase activity of 2-Cys Prdxs involves oxidation of the "peroxidatic" cysteine-thiolate to sulfenate (SO^-), followed by the formation of a disulfide bond with a second "resolving" cysteine in an adjacent subunit. This Prdx-Prdx disulfide bond is subsequently reduced by thioredoxin (Trx)/thioredoxin reductase (TR) to complete the catalytic cycle (Figure 1A).[2] Thus, Prdxs reduce peroxides. However, Prdxs have other roles in protecting cells against oxidative damage. For example, oligomeric forms of Prdxs can act as chaperones, inhibiting the aggregation of proteins under stress conditions.[2] As described below, Prdxs also have important roles in promoting cell signaling in response to hydrogen peroxide (H_2O_2).

It is well established that H_2O_2 acts as a signaling molecule, initiating responses that protect against oxidative damage. H_2O_2 signals also regulate fundamental processes, such as cell growth, differentiation, and migration (for reviews, see Holmström et al.,[4] Hurd et al.,[5] and Veal et al.[6]). Critical to the specificity of this signaling function is H_2O_2's capacity to selectively oxidize specific protein-cysteine thiols and thus regulate the activity of targeted proteins, including transcription factors (for example, Delaunay et al.[7] and Dansen et al.[8]), protein tyrosine phosphatases (PTPs) (reviewed in Tonks[9]), and kinases (for example, Byrne et al.,[10] Hourihan et al.,[11] and Wani et al.[12]). However, Prdxs are so abundant that H_2O_2 is extremely unlikely to react with cysteines in target proteins before encountering the more highly reactive peroxidatic cysteine of a Prdx.[13] One solution to this problem is that the sulfenylated Prdx (Prdx-SO^-) formed when Prdx's peroxidatic cysteine reacts with H_2O_2 can act as the oxidant, forming a disulfide with a cysteine of a peroxide-targeted protein. This is exemplified by H_2O_2-regulated transcription factors, such as STAT3 in mammalian cells and AP-1-like transcription factors in yeast, where the formation of a transient disulfide complex with the peroxidatic cysteine of a Prdx initiates further oxidation events that regulate their

 Crown Copyright © 2023 Published by Elsevier Inc.
This is an open access article under the CC BY license (http://creativecommons.org/licenses/by/4.0/).

CellPress
OPEN ACCESS

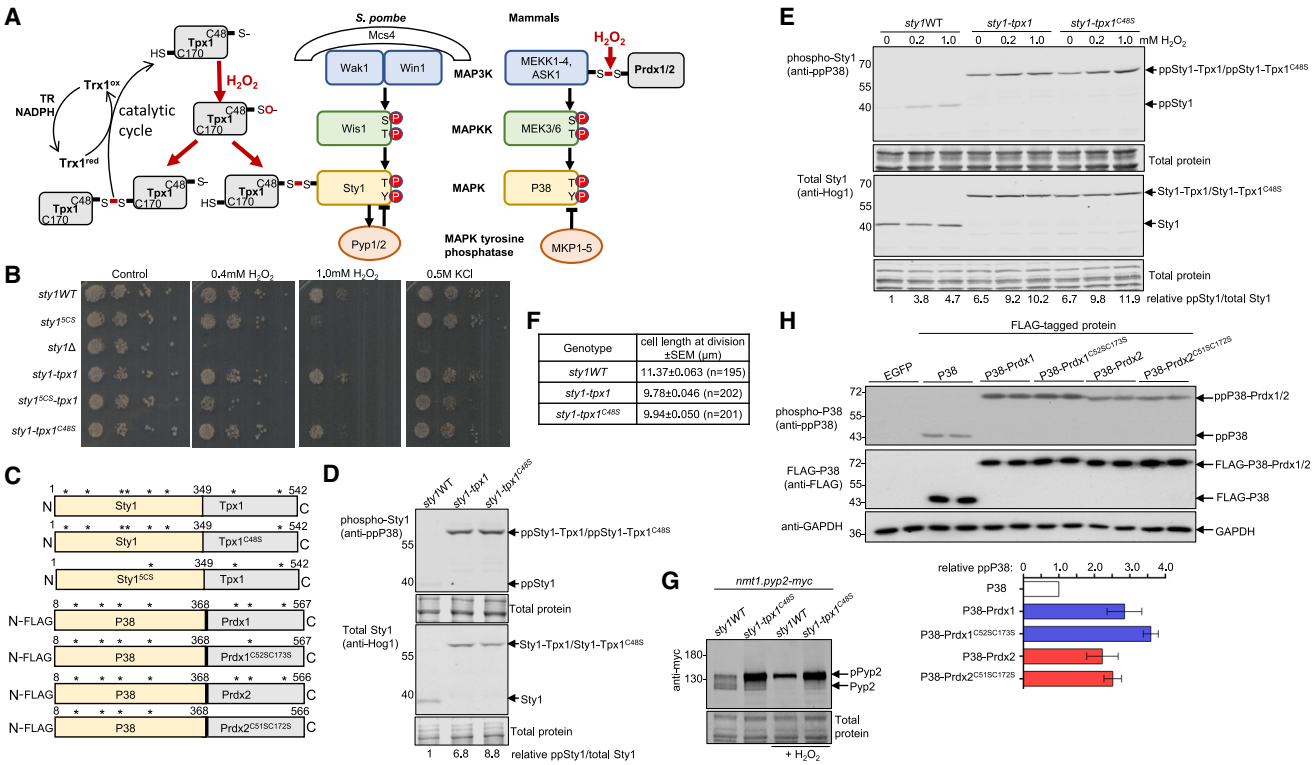

Figure1. Constitutive formation of complex with a Prdx increases phosphorylation and activity of P38 MAPK in yeast and human cells

(A) Left-hand side: the catalytic cycle of Prdx, exemplified by *S. pombe* Tpx1, involves the sulfenylated (SO^-) peroxidatic cysteine (C48) forming a disulfide bond with a resolving cysteine (C170) in another Tpx1 subunit that is reduced by thioredoxin ($Trx1^{red}$). Oxidized thioredoxin ($Trx1^{ox}$) is reduced by thioredoxin reductase (TR) using electrons from NADPH. Alternatively, Prdx can form disulfide bonds with cysteines in other proteins, for example, components of P38 MAPK signaling pathways, e.g., Sty1 (P38) or ASK1. Right-hand side: the activity of the *S. pombe* Sty1 and mammalian P38 mitogen-activated protein kinase (MAPK) is regulated by phosphorylation and dephosphorylation of conserved threonine (T) and tyrosine (Y) residues by MAPK kinases (MAPKK) and MAPK tyrosine phosphatases (MKP/Pyp), respectively. MAPK kinase kinases (MAP3K) activate MAPKK by phosphorylating conserved serine (S) and threonine (T) residues. Mcs4 is required for MAP3K activity in *S. pombe*.

(B) Growth of equal numbers of exponentially growing *sty1WT* (AD38), *sty1^{5CS}* (AD84), Δ*sty1* (JM1160), *sty1-tpx1* (MG17), *sty1^{5CS}-tpx1* (MG23), and *sty1-tpx1^{C48S}* (MG18) cells serially diluted and spotted on to YE5S plates containing H_2O_2, or 0.5 M KCl, and incubated at 30°C for 3 days.

(C) Diagram illustrating Sty1-Tpx1 and P38α-Prdx fusion protein constructs. Yellow, MAPK; gray, Prdx; and black, linking amino acids. *indicates cysteines present.

(D and E) Immunoblot analysis of cells expressing *sty1*WT (AD38), *sty1-tpx1* (MG17), and *sty1-tpx1^{C48S}* (MG18) before and following 10 min exposure to the indicated concentrations of H_2O_2. Antibodies against the dual TGY motif phosphorylated P38 (anti-ppP38) were used to detect phosphorylated Sty1 or Sty1-Tpx1 fusion proteins and total Sty1/Sty1-Tpx1 levels using anti-Hog1 antibodies. Total protein stain indicates protein loading, and molecular weight (MW) (kDa) marker positions are indicated. The relative levels of phosphorylated Sty1/total Sty1 are shown below each lane.

(F) Septating cells expressing *sty1-tpx1* (MG17) or *sty1-tpx1^{C48S}* (MG18) were significantly shorter than *sty1*WT (AD38) cells with p value < 0.0001 (t test); n = number of cells in each group.

(G) Immunoblotting analysis of the Sty1-stabilized substrate, Pyp2, in *sty1WT* (EB15)- or *sty1-tpx1^{C48S}* (EB16)-expressing cells co-expressing myc-tagged Pyp2 from the Sty1-independent *nmt1* promoter[3] before and after 30 min exposure to 1.0 mM H_2O_2.

(H) Phosphorylation of P38 in HEK-293T cells ectopically expressing enhancedGFP (control), FLAG epitope-tagged P38, P38-Prdx1, P38-Prdx2, or P38-Prdx fusion proteins in which the indicated cysteines in Prdx1 or 2 are serine-substituted. The graph shows the mean relative phosphorylation of each protein compared with total protein (anti-FLAG) ± standard deviation for the two biological repeats shown. See also Figures S1 and S2.

activity.[7,14–16] This signaling function does not require the resolving cysteine and thioredoxin peroxidase activity of the Prdx. However, the thioredoxin peroxidase activity of Tpx1, the single 2-Cys Prdx and homolog of mammalian Prdx1 and Prdx2 in the fission yeast, *Schizosaccharomyces pombe* (*S. pombe*), is essential for H_2O_2-induced activation of the AP-1-like transcription factor Pap1.[17–19] This is because the catalytic cycling of Prdx/Tpx1 as it reduces H_2O_2 also promotes the oxidation of thioredoxin (Trx) and other thioredoxin family proteins (Figure 1A). Thioredoxins reduce protein disulfides in many other proteins, including the intramolecular disulfides in active Pap1.[18,20] Consequently, as abundant thioredoxin substrates, Prdxs act as H_2O_2-dependent indirect inhibitors of other enzymes that require reduced thioredoxin for their activity under physiological conditions.[20–23]

P38 mitogen-activated protein kinases (MAPKs) are activated in response to a variety of different stimuli, including H_2O_2.[24,25] Canonical mechanisms of P38 activation involve regulation of

protein kinases and phosphatases, which modulate phosphorylation within the "TGY" motif of the kinase activation segment (Figure 1A). The direct regulation of "upstream" MAPK kinases (MAPKKs) and autophosphorylation and Arg-methylation of P38 itself have been proposed to control the signaling outputs of P38.[24,26,27] The *S. pombe* P38-related Sty1 MAPK (also known as Spc1) regulates both the timing of mitosis and transcriptional programs that allow cells to adapt to different growth conditions. Sty1 is activated by a wide range of environmental stimuli.[28–30] Interestingly, the *S. pombe* Prdx Tpx1 is specifically required for the activation of Sty1/P38 by H_2O_2.[31] Prdxs are also important for activating P38 MAPK in Metazoa.[32–36] In mammals, the Prdx Prdx1 has been proposed to instigate P38 activation by promoting the disulfide bond-mediated oligomerization and activation of Ask1, an upstream Ser/Thr MAPK kinase kinase (MAP3K).[35] Intermolecular disulfides formed between Prdx2 and MAP3Ks have also been implicated in the activation of P38 in human and *Drosophila* cells.[32] Intriguingly, H_2O_2-induced disulfides also form between the peroxidatic cysteine in Tpx1 and cysteines in Sty1.[31] However, the role that Tpx1-Sty1 disulfide complexes play in promoting Sty1 (P38) phosphorylation remains unclear. Indeed, despite intense scrutiny, we have been unable to find any evidence that Sty1-Tpx1 disulfides are an intermediate in the generation of intramolecular or intermolecular disulfides between cysteines in Sty1, as previously described for Yap1, STAT3, and ASK1.[7,15,35]

In this paper, we tested an alternative hypothesis: that directed formation of a complex with Tpx1/Prdx might be sufficient to increase Sty1/P38 phosphorylation. We undertook a genetically encoded proximity fusion approach, similar to that used to evaluate the function of covalently linked interactions with ubiquitin-like proteins, such as SUMO,[37] and the effect of physical constraints on signaling outputs from Protein kinase A (PKA) holoenzymes within signaling "islands."[38] Using this approach, we reveal that constitutive formation of a complex with a Prdx is sufficient to activate P38 MAPK in yeast and human cells, even in the absence of any activating stimuli. Notably, we find that the peroxide-reacting cysteine of the Prdx is dispensable for the increased activity of these P38-Prdx complexes. Instead, our experiments in yeast suggest that the Prdx-MAPK fusion protein (Tpx1-Sty1) provides a scaffold, supporting increased phosphorylation of canonical and non-canonical sites within the MAPKK and driving cells into mitosis. Our data suggest that the thioredoxin peroxidase activity of Tpx1 independently increases H_2O_2-induced Sty1/P38 phosphorylation by promoting the oxidation of the MAPK phosphatase (MKP) Pyp1. Together, we propose that these two complementary mechanisms permit fission yeast to "stock take" their reductive capacity to tailor MAPK-dependent responses, including the timing of entry into mitosis, according to the level of oxidative stress.

RESULTS

Multiple cysteines in Sty1 (P38) are involved in Tpx1-Sty1 disulfides and important for Sty1 activity

Following the exposure of cells to H_2O_2, disulfide complexes form between the invariant peroxidatic residue (C48) of the Prdx, Tpx1, and the P38 MAPK, Sty1 (Figure 1A).[31] Our previous work identified that cys35 in Sty1 was important for formation of one of these disulfide complexes.[31] However, Tpx1-Sty1 disulfide complexes still form in cells expressing $Sty1^{C35S}$, either ectopically[31] or from the *sty1* chromosomal locus (Figure S1A). Moreover, overexpression of Tpx1 stimulated increased H_2O_2-induced phosphorylation of $Sty1^{C35S}$ on the key regulatory Thr/Tyr residues in the activation segment ("TY" depicted in Figure 1A) revealing that the effect of Tpx1 on Sty1 activation was not solely dependent on C35 in Sty1 (Figure S1B). Intriguingly, five of six Sty1 cysteines are predicted to be surface accessible to react with H_2O_2/Tpx1, with only C202 required for Sty1 stability.[39] Indeed, only in cells expressing a Sty1 mutant in which these five cysteines were all substituted with serine ($Sty1^{5CS}$), was Sty1-Tpx1 disulfide formation abrogated (Figure S1C).

Sty1 activity is important for determining the timing of cell entry into mitosis; Δ*sty1* cells take significantly longer to pass through G2 than wild-type cells and thus grow to a longer cell length before they divide.[28,29] Our analysis revealed that $Sty1^{5CS}$-mutant-expressing cells were longer at the point of division than wild-type cells, strongly suggesting that $Sty1^{5CS}$'s pro-mitotic function was compromised (Figures S1D and S1E). Sty1 activity is also required for maintenance of the MKP Pyp1.[40] Consistent with lower Sty1 activity, $Sty1^{5CS}$-expressing cells contained less Pyp1 than wild-type cells (Figure S1F). This likely explains the slightly elevated phosphorylation of $Sty1^{5CS}$ (Figure S1G). Sty1 is vital for adaptation/survival under a number of different stress conditions, including osmotic and oxidative stress.[28,29] $Sty1^{5CS}$-expressing cells were able to adapt to osmotic stress but were less tolerant than wild-type cells to higher levels of H_2O_2 (Figure 1B). Together, these data suggest that cysteines involved in Sty1-Tpx1 disulfides are important for Sty1 activity under physiological and oxidative stress conditions, including a negative feedback mechanism regulating Pyp1 levels (Figures 1B and S1D–S1F).

Constitutive formation of complex with a Prdx increases phosphorylation of *S. pombe* Sty1 and human P38 MAPK

Next, we evaluated whether constitutive formation of a complex between Tpx1 and Sty1 was sufficient to activate Sty1. To do this, we engineered cells to express Sty1-Tpx1 fusion proteins from the Sty1 chromosomal locus, in place of wild-type Sty1 (Figure 1C). We also generated cells expressing a Sty1-$Tpx1^{C48S}$ fusion protein, in which the peroxide-reacting cysteine that becomes engaged in Sty1-Tpx1 disulfides[31] (see Figure 1A) was substituted with serine (Figure 1C). Crucially, both Sty1-Tpx1 fusions were expressed at similar levels to wild-type Sty1 and supported growth under stress conditions, confirming retention of Sty1 function (Figures 1B and 1D). By contrast, the oxidative stress sensitivity and lower Pyp1 levels in cells expressing a $Sty1^{5CS}$-Tpx1 fusion protein, provided further evidence that cysteines in Sty1 are required for Sty1 function independently from forming disulfide-bonded complexes with Tpx1 (Figures 1B and S1F).[39]

Strikingly, Sty1 phosphorylation was increased in cells expressing either Sty1-Tpx1 or Sty1-$Tpx1^{C48S}$ (Figure 1D) and to a similar extent to that observed in cells exposed to levels of H_2O_2 that stimulate Sty1-Tpx1 disulfide formation (Figures 1E,

S1A, and S1C).[31] It was possible that the increased phosphorylation of the Sty1-Tpx1 and Sty1-Tpx1^{C48S} fusion proteins reflected impaired Sty1 activity and thus reduced feedback inhibition by Sty1-regulated MKPs Pyp1 and Pyp2.[3,40] However, there was no less Pyp1 in cells expressing either Sty1-Tpx1 or Sty1-Tpx1^{C48S} fusion proteins (Figures S1F and S1H). Nevertheless, it was important to establish whether the increased phosphorylation of Sty1-Tpx1 and Sty1-Tpx1^{C48S} (Figures 1D and 1E) was correlated with increased Sty1 activity. Increased Sty1 catalytic activity is associated with a decrease in cell size at division, resulting from an accelerated entry into mitosis.[28,29] Therefore, we examined the length at which cells expressing wild-type or Sty1-Tpx1 fusion proteins divided. This revealed that Sty1-Tpx1- and Sty1-Tpx1^{C48S}-expressing cells both divided at a significantly smaller size than wild-type cells (Figure 1F). Importantly, this indicated that constitutive formation of a complex with Tpx1 increased Sty1 activity (Figure 1F). Next, we examined how expression of a Sty1-Tpx1^{C48S} fusion affected the phosphorylation of a Sty1 substrate, the MKP Pyp2, which is stabilized by Sty1-dependent phosphorylation.[3] As expected and consistent with Sty1-dependent phosphorylation, H_2O_2-treatment was required to shift the mobility of Pyp2 in wild-type cells (Figure 1G). By contrast, cells expressing Sty1-Tpx1^{C48S} contained substantially increased levels of lower mobility and phosphorylated Pyp2 (p-Pyp2), even prior to addition of H_2O_2. Together these data strongly support the conclusion that the Sty1-Tpx1 and Sty1-Tpx1^{C48S} fusion proteins are constitutively hyperactive compared with wild-type Sty1 (Figures 1F and 1G).

Prdxs also stimulate H_2O_2-induced activation of P38 MAPK in animals.[33,35] Moreover, although P38-Prdx disulfides have not been reported in mammalian cells, Prdxs have been shown to form disulfide complexes with kinases upstream of P38[32,35] (Figure 1A). Thus, we tested whether constitutive fusion of P38 to the cytosolic Prdx1 or Prdx2 was able to activate P38 in human cells by transfecting plasmids expressing FLAG epitope-tagged P38 (p38α/MAPK14) or the indicated P38-Prdx fusion proteins (Figure 1C). Importantly, P38-Prdx1 and P38-Prdx2 fusions were expressed at similar levels to P38 and able to phosphorylate a model P38 peptide substrate *in vitro* (Figures 1H and S2). As expected, phosphorylation of P38 at the key regulatory TY residues was very low under normal culture conditions. However, the phosphorylation of both P38-Prdx1 and P38-Prdx2 fusions was significantly increased (Figure 1H). This indicated that formation of a complex with a Prdx is sufficient to increase the phosphorylation of human P38. Strikingly, neither the peroxide-reacting nor resolving cysteine of Prdx1 or Prdx2 were required for the enhanced phosphorylation of p38-Prdx fusion proteins (Figure 1H). Although these experiments were unable to establish how P38-Prdx complexes' activity was affected, importantly, they suggested that P38-Prdx complexes can also increase P38 phosphorylation by a non-redox mechanism(s) in human cells.

Tpx1 (Prdx) promotes Sty1 (P38) activation independently of both MAP3K and a redox-sensitive cysteine in the MAPKK Wis1

To investigate the mechanism(s) by which P38-Prdx complexes increase P38 activity, we focused on identifying how Sty1-Tpx1 complexes activate *S. pombe* Sty1. This allowed us to take advantage of the presence of a single P38 MAPK, Sty1, and the cell-cycle phenotypes associated with altered Sty1 activity,[28,29] including the shortened G2 (reflected in decreased cell length at division) observed in cells expressing Sty1-Tpx1 in place of Sty1 (Figure 1F). We also exploited mutants in which genes encoding other pathway components (depicted in Figure 1A) were deleted or engineered to express mutant versions from their native promoter and chromosomal locus. In contrast to the redundancy of mammalian MKK3 and MKK6, a single MAPKK, Wis1, phosphorylates Sty1[28–30] (Figure 1A). We previously demonstrated that overexpression of Tpx1 restores peroxide-inducible Sty1 phosphorylation to cells expressing a phospho-mimetic Wis1 mutant (Wis1^{DD}), in which the canonical MAP3K-phosphorylated sites, Ser469 and Thr473 ("S and T" indicated in Figure 1A), are substituted with aspartate.[31] This suggested that overexpression of Tpx1 does not stimulate H_2O_2-dependent Sty1 phosphorylation by increasing MAP3K-dependent activation of Wis1. To test whether Sty1-Tpx1 also increased Sty1 phosphorylation independently from MAP3K-dependent activation of Wis1, we attempted to construct a strain co-expressing Sty1-Tpx1 and the phospho-mimetic Wis1^{DD} mutant. However, less than 10% of viable spores obtained from a cross between the two strains bore markers indicating the presence of both alleles (rather than the expected 25% for unlinked genes). Sty1 activity is tightly regulated such that Wis1 overexpression is lethal.[29] Hence, the lower viability of cells co-expressing *sty1-tpx1* and *wis1^{DD}* suggested a synthetic negative interaction, with both alleles acting independently to increase Sty1 phosphorylation to lethal levels. Indeed, our examination indicated that "*sty1-tpx1 wis1^{DD}*" strains, which genotypically bore both alleles, had adapted to the deleterious effect of hyperactivated Sty1 by lowering Sty1 expression to such an extent that they exhibited the long cell phenotype associated with its loss (Figures S3A and S3B). Interestingly, a cysteine in Wis1, C458, was recently proposed to be sensitive to oxidation and involved in regulating Wis1 activity.[41] However, ectopic overexpression of Tpx1 (Figure S3C) and expression of Sty1-Tpx1 fusion protein (Figure S3D) both caused similar increases in Sty1 phosphorylation in cells expressing either Wis1^{C458S} or wild-type Wis1. Thus, it was unlikely that altered oxidation or elevated MAP3K-dependent phosphorylation of Wis1 mediated the effect/s of Tpx1 on Sty1 phosphorylation. Taken together these data strongly suggested that Sty1-Tpx1 complexes and overexpression of Tpx1 increased phosphorylation of Sty1 by a novel MAP3K-independent mechanism(s).

High levels of Tpx1 promote H_2O_2-induced Sty1 phosphorylation by increasing the thioredoxin-dependent oxidation of the MAPK tyrosine phosphatase Pyp1

The utilization of a deprotonated cysteine in the catalytic site of PTPs renders them sensitive to inhibition by peroxide-induced oxidation.[9] Hence, we considered the possibility that Tpx1 increased H_2O_2-induced Sty1 activation by promoting the oxidation of Pyp1 and/or Pyp2, the MKPs responsible for deactivating Sty1.[28] First, we tested whether Pyp1 or Pyp2 were required for the increased H_2O_2-induced Sty1 phosphorylation in cells

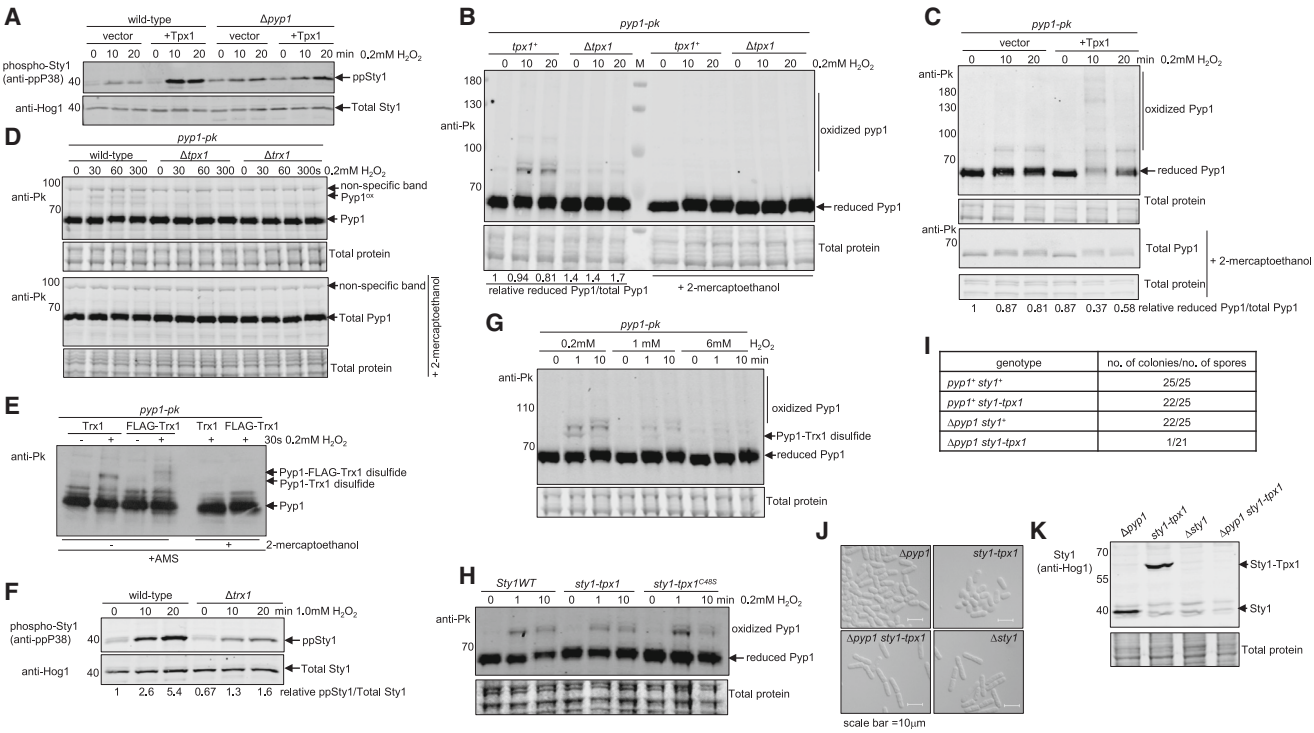

Figure 2. High levels of Prdx (Tpx1) promote H_2O_2-induced P38 (Sty1) phosphorylation by promoting the thioredoxin-dependent oxidation of the MAPK tyrosine phosphatase Pyp1

(A) Immunoblot analysis of Sty1 phosphorylation (anti-ppP38) in wild-type (CHP429) or Δ*pyp1* (NJ102) cells harboring vector (Rep1) or Rep1*tpx1*$^+$ before and following 10 or 20 min exposure to 0.2 mM H_2O_2. Total Sty1 was detected with anti-Hog1.

(B–F) Immunoblot analysis of Pyp1 oxidation state in cells expressing Pk-tagged Pyp1 (Pyp1-3pk) detected with anti-Pk antibodies in the following: (B) wild-type *tpx1*$^+$ (AD142) and Δ*tpx1* (AD143) and (C) wild-type cells (HL2) harboring vector (Rep1) or Rep1*tpx1*$^+$ before and following treatment with 0.2 mM H_2O_2 for 0, 10, and 20 min. Samples reduced with 2-mercaptoethanol were used to determine "total Pyp1." The relative levels of "reduced Pyp1" normalized to "total Pyp1" are shown. (D) Wild-type (AD142), Δ*tpx1* (AD143), and Δ*trx1* (AD130) cells before or after exposure to 0.2 mM H_2O_2 for up to 5 min. Oxidized Pyp1 (Pyp1^{ox}) present only in wild-type cells (upper panel) was not detected when samples were reduced with 2-mercaptoethanol prior to electrophoresis (lower panel). (E) Wild-type Trx1 (AD142) or FLAG-tagged Trx1 (AD144) before or after 30 s exposure to 0.2 mM H_2O_2. The sensitivity of the band with lower mobility in FLAG-Trx1-expressing cells to 2-mercaptoethanol treatment confirms that it represents a Trx1-Pyp1 disulfide complex. Protein-cysteine thiols were reacted with 4-acetamido-4′-maleimidylstilbene-2,2′-disulfonic acid (AMS) during solubilization step. (F) Sty1 phosphorylation (anti-ppP38) in wild-type (AD142) or Δ*trx1* (AD130) cells before and following 10 or 20 min exposure to 1.0 mM H_2O_2. Total Sty1 was detected with anti-Hog1. Relative levels of Sty1 phosphorylation are shown.

(G and H) Immunoblot analysis (anti-Pk) of wild-type (MC2), *sty1-tpx1* (MC12), and *sty1-tpx1*^{C48S} (MC82) cells expressing Pk-tagged Pyp1 (Pyp1-3pk) before and following exposure, as indicated, to 0.2, 1.0, or 6.0 mM H_2O_2 for 1 or 10 min. Oxidized Pyp1 forms are indicated.

(I) Analysis of dissected tetrads from a cross between Δ*pyp1 sty1*$^+$ (NJ102) and *pyp1*$^+$ *sty1-tpx1* (MG17) cells showing the fraction of viable spores with each genotype (colonies formed/total number of spores).

(J) Differential interference contrast (DIC) light microscopy of exponentially growing Δ*pyp1* (NJ102), *sty1-tpx1* (MG17), and Δ*pyp1 sty1-tpx1* (MC150) cells in comparison with a Δ*sty1* (JM1160). Scale bar represents 10μm.

(K) Immunoblotting analysis of Δ*pyp1 sty1*$^+$ (NJ102) and *sty1-tpx1 pyp1*$^+$ (MG17) Δ*sty1* (JM1160), and Δ*pyp1 sty1-tpx1* (MC150) with anti-Hog1 antibodies demonstrated that Sty1-Tpx1 fusion protein was undetectable in the single isolate of Δ*pyp1 sty1-tpx1* cells (MC150) obtained from crossing NJ102 and MG17. See also Figure S3.

overexpressing Tpx1.[31] As expected, Sty1 phosphorylation was increased in Δ*pyp1* mutant cells, confirming the importance of this phosphatase in maintaining low levels of Sty1 activity (Figure 2A).[28,29] However, there was no significant increase in Sty1 phosphorylation in Δ*pyp1* cells in response to H_2O_2, even with overexpression of Tpx1 (Figures 2A and S3E). By contrast, overexpression of Tpx1 increased H_2O_2-induced Sty1 phosphorylation in wild-type cells and also restored some H_2O_2-inducibility to Sty1 phosphorylation in Δ*pyp2* cells (Figures 2A and S3E). This suggested that increased Tpx1 levels might increase H_2O_2-induced Sty1 phosphorylation by promoting the oxidation and inactivation of Pyp1. To test this hypothesis, we examined the effect of Tpx1 and H_2O_2 on Pyp1. This revealed the presence of several slower-migrating forms of Pyp1 following the exposure of wild-type cells to H_2O_2 (Figure 2B). Although a small shift in Pyp1 mobility reflecting stress-induced phosphorylation remained, other slower-migrating forms were absent when samples were reduced with 2-mercaptoethanol prior to SDS-PAGE. This identifies them as oxidized forms of Pyp1 (Figure 2B and lower panels of Figures 2C and 2D). Notably, these oxidized forms of Pyp1 were not detected in Δ*tpx1* mutant cells, suggesting that Tpx1 was required for their formation (Figures 2B and

2D). Conversely, the H_2O_2-induced oxidation of Pyp1 was dramatically increased in cells overexpressing Tpx1, such that levels of reduced Pyp1 were transiently depleted to less than 50% of total Pyp1 (Figure 2C). These data suggest that Tpx1 promotes reversible H_2O_2-induced oxidation of Pyp1 into slower-migrating, disulfide-bonded complexes. Importantly, the correlation between the H_2O_2-induced formation of these complexes and increased Sty1 phosphorylation suggested these complexes lowered Pyp1's activity toward Sty1 (Figures 2A–2C).

Next, we explored the role Tpx1 plays in Pyp1 oxidation. First, we determined that the most rapidly induced complex (~84 kDa) was maximally detected within 30 s following exposure of wild-type cells to 0.2 mM H_2O_2 (Figure 2D). Intriguingly, our analysis of Δ*trx1* mutant revealed that thioredoxin (Trx1) was required for the formation of Pyp1 disulfide complexes (Figure 2D). Although it was possible that Tpx1 acted as a direct redox transducer, thioredoxin family proteins also form disulfide complexes with protein PTPs that have been proposed to be important for redox-regulation of PTP activity.[42,43] Indeed, the mobility (~84 kDa) of this H_2O_2-induced complex was consistent with that expected for a disulfide between Pyp1-3pk (72 kDa) and Trx1 (11.3 kDa) (Figures 2B–2D).[42,43] Furthermore, in cells expressing FLAG epitope-tagged Trx1 instead of wild-type Trx1, the mobility of the most prominent oxidized (2-mercaptoethanol-sensitive) Pyp1 species was decreased, as expected for a disulfide complex between Pyp1 and FLAG-tagged Trx1 (Figure 2E).

The nature of the other slower-migrating oxidized Pyp1 forms (Figures 2B and 2C) remains to be established. However, the formation of intermolecular disulfide-bonded oligomers has been shown to inhibit other PTPs, including a MKP, HePTP, that dephosphorylates p38α.[44] Consistent with Pyp1 oxidation providing a similar mechanism to reversibly inhibit Pyp1 and activate Sty1, there was a much smaller H_2O_2-induced increase in Sty1 phosphorylation in Δ*trx1* mutant cells, where H_2O_2-induced Pyp1 disulfides were not detected (Figures 2D and 2F).

Accordingly, these data were consistent with the thioredoxin peroxidase activity of Tpx1 stimulating the Pyp1 oxidation indirectly by promoting the oxidation of Trx1: in cells exposed to these (≤ mM) levels of H_2O_2, Tpx1-Tpx1 disulfides are the most abundant Trx1 substrate, and TR activity is limiting, such that the pool of Trx1 becomes transiently oxidized.[20] Therefore, increased Tpx1 activity would be expected to increase Pyp1 disulfide complex formation, as observed in cells overexpressing Tpx1 (Figure 2C). Consistent with this, Pyp1-Trx1 disulfides were less abundant following exposure of cells to higher concentrations of H_2O_2 (≥1 mM), at which Tpx1 is hyperoxidized and more reduced thioredoxin is available (Figure 2G).[20] Notably, the majority of Pyp1 remained resistant to disulfide formation, even following exposure to 6 mM H_2O_2 (Figure 2G). Importantly, this suggested that additional mechanisms were responsible for the more substantial increase in Sty1 phosphorylation observed in cells exposed to these higher concentrations of H_2O_2.[31,45,46]

Sty1-Tpx1 (P38-Prdx) complexes increase Sty1 activity independently from H_2O_2/Tpx1/Trx1-dependent regulation of Pyp1

Although it was possible that the constitutive phosphorylation of Sty1-Tpx1 fusion proteins reflected increased Pyp1 oxidation, Pyp1 was oxidized to a similar extent in cells expressing wild-type Sty1, Sty1-Tpx1, or Sty1-Tpx1^{C48S} fusion proteins (Figure 2H). Moreover, when we crossed strains expressing Sty1-Tpx1 fusion and Δ*pyp1* mutant alleles, we observed a very strong synthetic lethal interaction, with 95% of spores with a *sty1-tpx1* Δ*pyp1* genotype failing to give rise to a colony (Figure 2I and not shown). This strongly suggests that *sty1-tpx1* and Δ*pyp1* alleles act independently to increase Sty1 phosphorylation, thus increasing it to lethal levels when co-expressed. Indeed, analysis of colonies bearing markers of both alleles revealed that surviving cells had completely eliminated Sty1-Tpx1 expression and activity (Figures 2J and 2K and not shown). This very strong selection pressure to eliminate Sty1-Tpx1 expression suggests Pyp1 partially mitigates the physiological impacts of constitutive Sty1 activation in cells expressing Sty1-Tpx1/Sty1-Tpx1^{C48S} fusion proteins. Most importantly, these data strongly suggest that Sty1-Tpx1 complex formation can independently increase Sty1 activity aside from any effect of Tpx1 on Pyp1 oxidation state or activity.

High levels of H_2O_2 are required for maximal, MAP3K-dependent phosphorylation of the Wis1 MAPKK

The synthetic lethality of Sty1-Tpx1-expressing alleles with either a Δ*pyp1* deletion mutant or a *wis1^{DD}* mutant allele (Figures 2I–2K, S3A, and S3B) strongly suggested that Sty1-Tpx1 fusions increase Sty1 phosphorylation by MAP3K and phosphatase-independent mechanism/s. Wis1 is the only upstream MAPKK that phosphorylates Sty1 under physiological or stress conditions.[28,29] Therefore, we set out to investigate whether Sty1-Tpx1 impacted Wis1 activity. We began by establishing an assay to evaluate the activation of Wis1 by MAP3K-dependent phosphorylation. Using Phos-tag™ to enhance the separation of phosphorylated forms, we detected lower mobility Wis1 and Wis1^{DD} species (pWis1) in cells grown under non-stress conditions that were eliminated by phosphatase treatment (Figure S4A). Intriguingly, this suggested that Wis1 was phosphorylated under physiological conditions, on different (non-canonical) sites from those regulated by the MAP3K. As expected, there was a significant phosphatase-sensitive decrease in the mobility of wild-type Wis1 under osmotic stress conditions (pppWis1). However, unexpectedly, Wis1^{DD} also underwent a smaller, phosphatase-sensitive shift (ppWis1), suggesting that Wis1 undergoes additional stress-induced phosphorylation to the canonical phosphorylation catalyzed by the stress-activated MAP3Ks Wak1 and Win1 (Figure S4A).

Wis1^{DD} was also phosphorylated following oxidative stress, despite the absence of the canonical MAP3K phospho-sites (Figure S4B). However, the more pronounced shift in wild-type Wis1 mobility (pppWis1) following exposure to osmotic stress (0.6 M KCl) or high levels of H_2O_2 (6 mM) suggested this electrophoretic retardation reflected phosphorylation of canonical MAP3K-phosphorylated residues (Figure S4B). As expected, this shift was also dependent on the presence of Mcs4, a fungal-specific scaffold protein required (as illustrated in Figure 1A) to support MAP3K (Win1 and Wak1) activity (Figure S4C).[47,48]

Notably, when we examined the response to different concentrations of H_2O_2, we were surprised to find that exposure to a much higher dose (≥1 mM) of H_2O_2 was required for Wis1

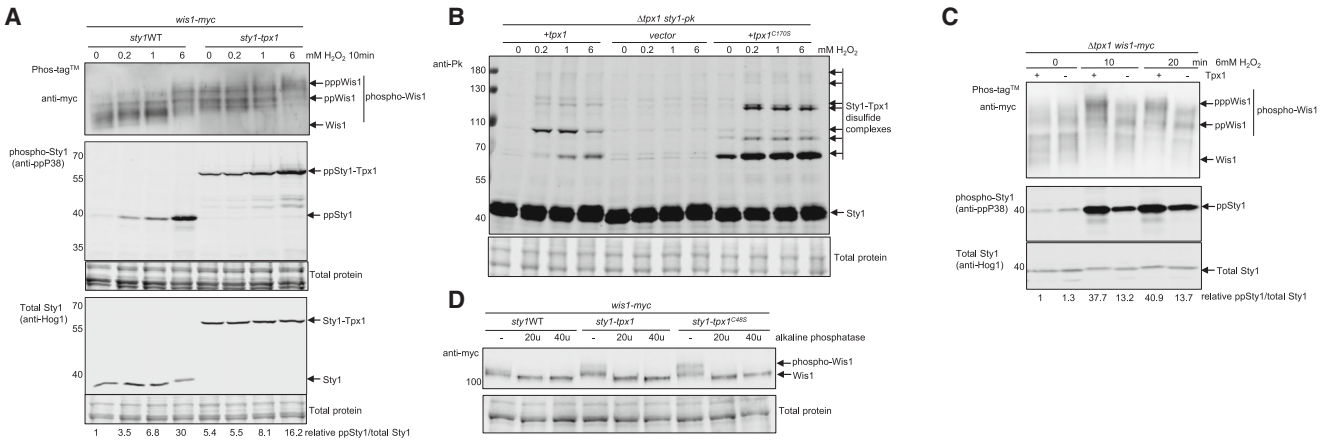

Figure 3. Tpx1 is required for H_2O_2-induced phosphorylation of the MAPKK Wis1 and Sty1-Tpx1 complexes promote constitutive Wis1 phosphorylation

(A) Immunoblotting analysis of Wis1 and Sty1 phosphorylation in cells expressing wild-type Sty1 (MC2) or Sty1-Tpx1 fusion protein (MC12) before and following 10 min exposure to increasing concentrations of H_2O_2. The lower mobility of phosphorylated Wis1 was detected by immunoblotting proteins separated using Phos-tag™ SDS-PAGE. The relative levels of dual TGY motif phosphorylated Sty1 (anti-ppP38)/total Sty1 (anti-Hog1) normalized to wild type (t = 0) are shown below each lane.

(B) Immunoblot analysis (anti-Pk) of Δ*tpx1* cells co-expressing Pk-tagged Sty1 (AD21) with wild-type Tpx1 (Rep1Tpx1) or Tpx1^{C170S} (Rep1Tpx1^{C170S}) before and following 10 min exposure to 0.2, 1, or 6 mM H_2O_2. Comparisons with vector control (Rep1) allow distinction of non-specific bands from Tpx1-Sty1 disulfide complexes.

(C) The phosphorylation of Wis1 and Sty1 in Δ*tpx1* cells (MC88) harboring vector (Rep1) or ectopically expressing Tpx1 from Rep1*tpx1*$^+$ before and after exposure of cells to 6 mM H_2O_2. The relative levels of dual TGY motif phosphorylated Sty1 (anti-ppP38)/total Sty1 (anti-Hog1) normalized to wild type (t = 0) are shown below each lane.

(D) Comparison of the mobility of Wis1 in extracts from cells expressing wild-type Sty1 (MC2), *sty1-tpx1* (MC12), or *sty1-tpx1*^{C48S} (MC82) before and after treatment with alkaline phosphatase. The phosphatase-sensitivity of the less mobile Wis1 forms suggests the shift/s reflect increased Wis1 phosphorylation in Sty1-Tpx1 expressing cells. The positions of MW markers separated on conventional gels are indicated (kDa). See also Figure S4.

hyperphosphorylation (pppWis1) than was required to activate Sty1 (compare Figures 3A, 1E, and S4D). Thus, although Wis1 undergoes multiple phosphorylation events, our data suggest that phosphorylation on MAP3K sites only increases significantly following exposure of wild-type cells to concentrations of $H_2O_2 \geq 1$ mM. This suggested that the Tpx1-dependent oxidation of Pyp1 (Figure 2) and Tpx1-Sty1 disulfide complexes formed in response to 0.2–1 mM H_2O_2 (Figure S1A) could be critically important for activation of Sty1 by these lower levels ($\leq$1 mM).

Tpx1 is required for H_2O_2-induced Wis1 phosphorylation and Sty1-Tpx1 complexes increase Wis1 phosphorylation

Next, we investigated whether Tpx1-Sty1 complexes affected Wis1 phosphorylation. Tpx1 is required for H_2O_2-induced activation of Sty1, over a range of concentrations up to 10 mM H_2O_2.[31] Moreover, Tpx1-Sty1 disulfide complexes formed in response to a wide range of H_2O_2 concentrations (0.2–6 mM), including those at which Wis1 undergoes MAP3K-dependent phosphorylation (Figure 3B). Indeed, our analysis of Δ*tpx1* mutant cells indicated that Tpx1 was important for maximal Wis1 phosphorylation (pppWis1) in response to 6 mM H_2O_2 (Figures 3C, S4E, and S4F). Next, we examined whether Wis1 phosphorylation was affected in cells expressing Sty1-Tpx1 fusion proteins. Strikingly, this revealed that in cells expressing Sty1-Tpx1 fusion proteins, Wis1 was hyperphosphorylated to less electrophoretically mobile forms even in the absence of stress (Figures 3A and 3D). Significantly, these data suggest that Sty1-Tpx1 complex formation is sufficient to promote hyperphosphorylation of Wis1.

Wis1 is regulated by MAP3K-independent autophosphorylation

Intriguingly, our data suggested that Wis1 undergoes multiple stress-induced phosphorylation events promoted by expression of Sty1-Tpx1 fusion proteins (Figures 3 and S4). To further investigate how Wis1 phosphorylation is regulated, we made use of a chemical genetic approach using Δ*pyp1*Δ*pyp2* cells expressing Wis1^{DD} and an ATP analog-sensitive Sty1 mutant (Sty1^{T97A}). The viability of these cells is maintained by inhibiting Sty1 kinase activity with the ATP analog, 3-BrB-PP1.[49] We observed a small, but reproducible, stress-induced decrease in Wis1^{DD} mobility in these cells, corroborating that Wis1 undergoes a stress-induced phosphorylation on different sites from those phosphorylated by the MAP3K (Figures 4A, S5A, S4A, S4B, and S4F). Significantly, this stress-induced increase in Wis1^{DD} phosphorylation was mirrored by stress-induced increases in Sty1 phosphorylation, strongly suggesting that it increases Wis1 activity (Figure 4A).

Importantly, the possibility that stress-induced phosphorylation of Wis1^{DD} or Sty1 in this experiment involved inhibition of either Pyp1 or Pyp2 was eliminated because neither phosphatase was present in these cells (Figure 4A). Furthermore, the presence of 3-BrB-PP1, which inhibits the kinase activity of Sty1^{T97A}, did not prevent stress-induced Wis1^{DD} phosphorylation, indicating that

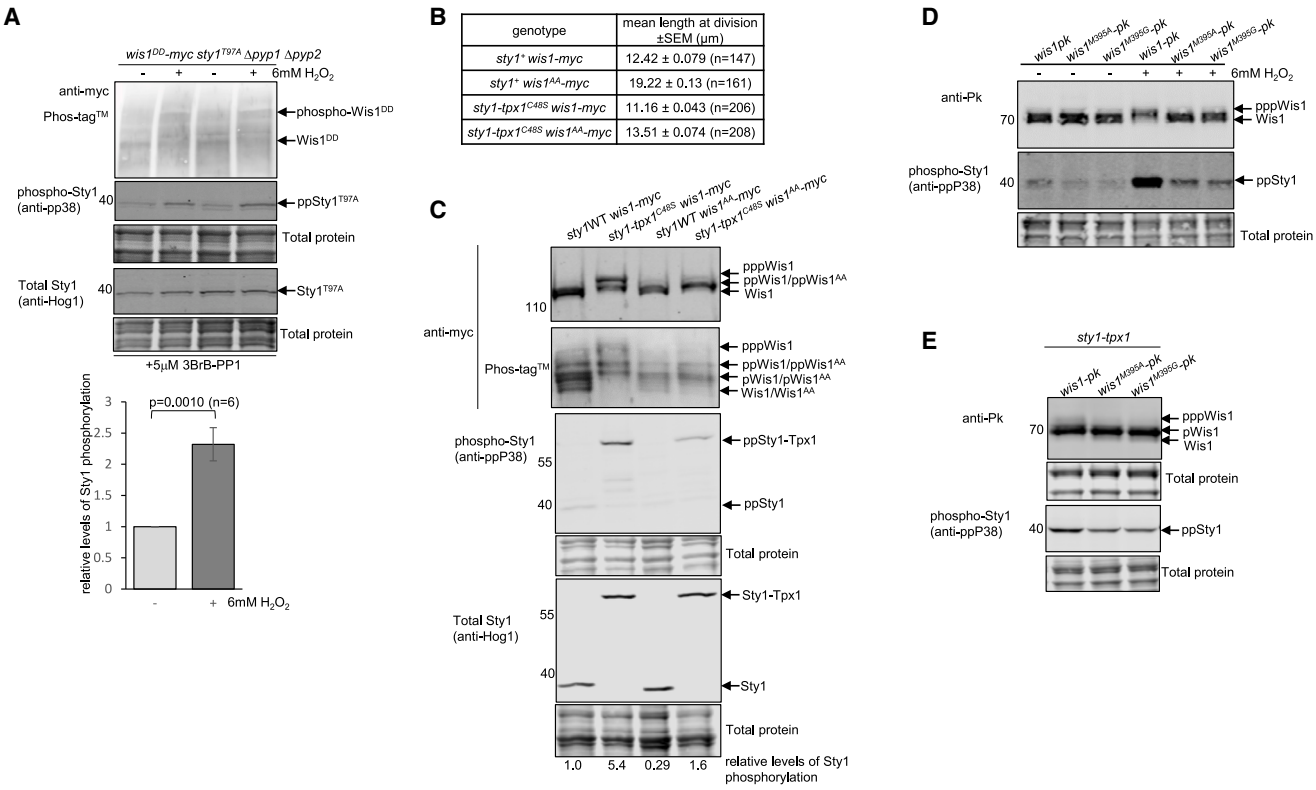

Figure 4. Wis1 undergoes autophosphorylation in response to stress or in presence of Sty1-Tpx1 complexes

(A) Immunoblot analysis of Wis1^{DD}.myc (anti-myc) on a Phos-tag™ gel, in Δ*pyp1* Δ*pyp2* Sty1^{T97A} (SISA[49]; KS8266 in lanes 1 and 2, KS8311 in lanes 3 and 4) cells grown throughout in media containing 5 μM 3-BrB-PP1 and treated, as indicated, for 10 min with 6 mM H_2O_2. Quantitative analysis of multiple experiments confirmed the small, stress-induced increase in Sty1 phosphorylation (anti-ppP38/anti-Hog1) was significant (t test p = 0.0010). Error bar represents the standard error of the mean (SEM) from 6 experiments.

(B and C) Expression of a Sty1-Tpx1 fusion is sufficient to rescue phenotypes associated with loss of MAP3K-dependent phosphorylation of Wis1. (B) Table shows the mean length of septating cells co-expressing wild-type Sty1 or Sty1-Tpx1^{C48S} fusion with wild-type Wis1 or Wis1^{AA}: *sty1*WT wis1-myc (MC132) *sty1*$^{+}$ *wis1*^{AA}*-myc* (MC122), *sty1-tpx1*^{C48S} (MC135), and *sty1-tpx1*^{C48S} wis1^{AA}*-myc* (MC130). (C) Immunoblotting analysis of proteins extracted from cells co-expressing Sty1 or *Sty1-Tpx1*^{C48S} with *Wis1-myc* (MC132 and MC135) or *Wis1*^{AA}-myc (MC122 and MC130). Proteins were separated by conventional or Phos-tag™ SDS-PAGE and analyzed with anti-myc, anti-ppP38, or anti-Hog1 antibodies. Arrows indicate fully phosphorylated Wis1 (pppWis1) and Wis1 phosphorylation outside of MAP3K sites (ppWis1/ppWis1^{AA} and pWis1/pWis1^{AA}). Relative levels of Sty1 phosphorylation (ppSty1/Total Sty1) are also shown.

(D and E) Immunoblotting analysis, with anti-Pk or anti-ppP38 antibodies, of proteins extracted from cells co-expressing wild-type Wis1-3pk, Wis1^{M395A}-3pk, or Wis1^{M395G}-3pk and (D) wild-type Sty1 (MG46, MG47, and MG48) before or following treatment for 10 min with 6 mM H_2O_2 or (E) Sty1-Tpx1 fusion protein (MG49, MG50, and MG51). See also Figure S6.

Sty1 kinase activity was not required (Figures 4A, S5A, and S5B).[49] Similarly, analysis of cells expressing analog-sensitive Sty1 fused to Tpx1 (Sty1^{T97A}-Tpx1) suggested that inhibiting the kinase activity of the fusion did not affect Wis1 phosphorylation (Figure S5C). Thus, we conclude that the stress-induced non-canonical phosphorylation of Wis1, which is also increased by Sty1-Tpx1 complexes, does not require Sty1's kinase activity.

Next, we co-expressed the Sty1-Tpx1^{C48S} fusion with a Wis1^{AA} mutant, in which the MAP3K-phosphorylated residues are substituted with alanine. Wis1^{AA} cells are significantly elongated, reflecting the mitotic delay associated with Sty1 hypophosphorylation (Figures 4B, 4C, and S6A).[50] Although expression of Sty-Tpx1^{C48S} stimulated a bigger increase in Sty1 activity in cells expressing wild-type Wis1, expression of Sty1-Tpx1^{C48S} also increased Sty1 phosphorylation and partially rescued the cell-cycle defect of Wis1^{AA} cells (Figures 4B and 4C). This was consistent with Sty1-Tpx1 increasing Wis1 activity independently from MAP3K-dependent phosphorylation. Moreover, in cells expressing Sty1-Tpx1^{C48S}, we observed a shift in the mobility of Wis1^{AA} consistent with this increased activity reflecting increased non-canonical phosphorylation (compare lanes 3 and 4 in Figure 4C).

Next, we explored whether Wis1 kinase activity might be important for the additional (non-canonical) phosphorylation detected following stress or Sty1-Tpx1 complex formation. To examine this possibility, we engineered cells expressing mutant versions of Wis1, Wis1^{M395G}, or Wis1^{M395A}, predicted to enlarge the ATP-binding pocket, rendering them sensitive to inhibition by the ATP analog 3-BrB-PP1.[51] Although, both Wis1^{M395G} and Wis1^{M395A} were expressed at wild-type levels, Sty1 phosphorylation was very low and minimally increased even in response to 6 mM H_2O_2 in these cells (Figure 4D). This suggested that the

A

genotype	Cell length at division (μm) ±SEM
sty1WT mcs4⁺	12.68±0.069 (n=180)
sty1WT Δmcs4	15.69±0.066 (n=250)
sty1-tpx1 mcs4⁺	10.70±0.041 (n=288)
sty1-tpx1 Δmcs4	10.70±0.047 (n=257)

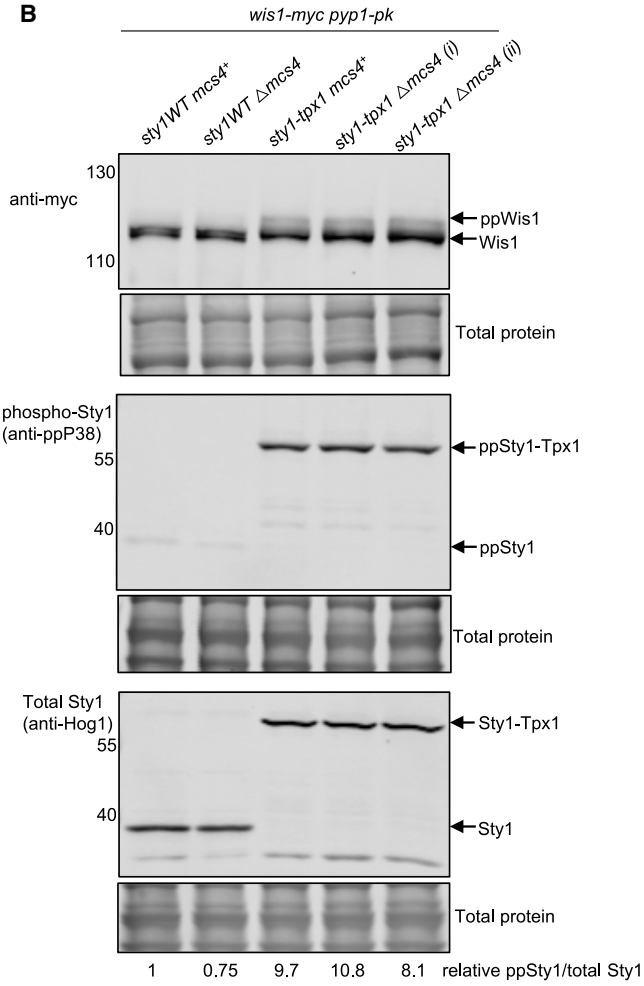

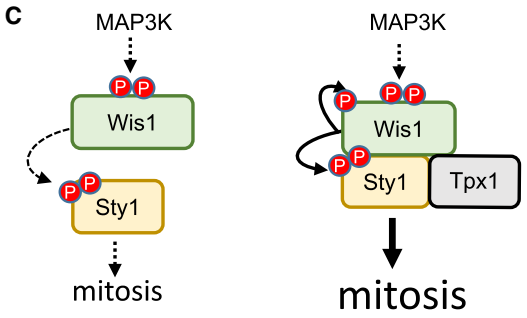

Figure 5. Sty1-Tpx1 complexes bypass the requirement for Mcs4 for phosphorylation of Wis1 and activation of Sty1

(A) Expression of Sty1-Tpx1 fusion protein rescues the long cell phenotype of *Δmcs4* cells; table shows the mean length of septating wild-type (MC2), *Δmcs4* (MC77), *sty1-tpx1* (MC12), and *sty1-tpx1 Δmcs4* (MC83) cells.

(B) Immunoblotting analysis of the phosphorylation and levels of Wis1 and Sty1 in cell lysates from wild-type (MC2), *Δmcs4* (MC77), *sty1-tpx1* (MC12), and two different *sty1-tpx1 Δmcs4* (MC83) strains (i and ii) expressing Wis1-12myc. Blots were analyzed with anti-myc, anti-ppP38, and anti-Hog1 antibodies and total protein stain. Relative levels of phosphorylated Sty1/total Sty1 indicated below each lane.

(C) Model illustrating how Tpx1-Sty1 complexes provides a scaffold/signaling platform supporting the stress-induced activation of Wis1 by MAP3K and autophosphorylation. Thus, constitutive "prdxylation" of the Sty1 MAPK accelerates entry into mitosis.

catalytic activity of both Wis1 mutant proteins was substantially lower, even in the absence of the ATP analog. Indeed, consistent with the requirement of Wis1-dependent phosphorylation of Sty1 for timely entry into mitosis, cells expressing Wis1^{M395G} or Wis1^{M395A} were elongated (Figure S6B). Strikingly, the stress-induced phosphorylation of Wis1^{M395G} and Wis1^{M395A} was also compromised, strongly suggesting that Wis1 kinase activity was required for the stress-induced phosphorylation and activation of Wis1 (Figure 4D). Similarly, the constitutive hyperphosphorylation of Wis1 (pppWis1) in cells expressing Sty1-Tpx1 fusion proteins was ablated in cells expressing either Wis1^{M395G} or Wis1^{M395A} (Figure 4E). These data suggest that Sty1-Tpx1 complex formation also promotes the autophosphorylation of Wis1.

Sty1-Tpx1 complexes support Wis1 activation in the absence of the Mcs4 scaffold protein

The ability of a constitutively formed complex between Tpx1 and Sty1 to increase Wis1 phosphorylation, even in the absence of stress, suggested that H_2O_2-induced Tpx1-Sty1 disulfide formation activates Wis1 and Sty1 concomitantly. Hence, we examined whether Sty1-Tpx1 complexes might generate a "signaling island," enhancing interactions between components of the Sty1 MAPK signaling pathway. Mcs4 is a fungal-specific protein that performs a scaffolding function, guiding the interaction of Wak1 and Win1 MAP3Ks with Wis1[47] (as depicted in Figure 1A). Consistent with this essential function in supporting Sty1 activation, Δ*mcs4* mutant cells are delayed in entry to mitosis, reaching a significantly longer size than wild-type cells before dividing (Figure 5A).[45,47,48] To test whether Tpx1 could also act as a signaling scaffold, we examined whether Sty1-Tpx1 complex formation could bypass the requirement for Mcs4 for MAP3K-dependent phosphorylation of Wis1. Remarkably, analysis of cells obtained from a cross between strains expressing *sty1-tpx1* or Δ*mcs4*, revealed that Sty1-Tpx1 expression stimulated similar levels of constitutive Wis1 phosphorylation in Δ*mcs4* mutant as in wild-type (*mcs4⁺*) cells (Figure 5B). Accordingly, there were similar levels of Sty1 phosphorylation in *sty1-tpx1 mcs4⁺* and *sty1-tpx1* Δ*mcs4* strains (Figure 5B). Moreover, loss of *mcs4* had no effect on the length of septating cells expressing Sty1-Tpx1, with both *sty1-tpx1 mcs4⁺* and *sty1-tpx1* Δ*mcs4* cells significantly shorter than wild type (Figure 5A). These data demonstrate that constitutive Sty1-Tpx1 complex formation is

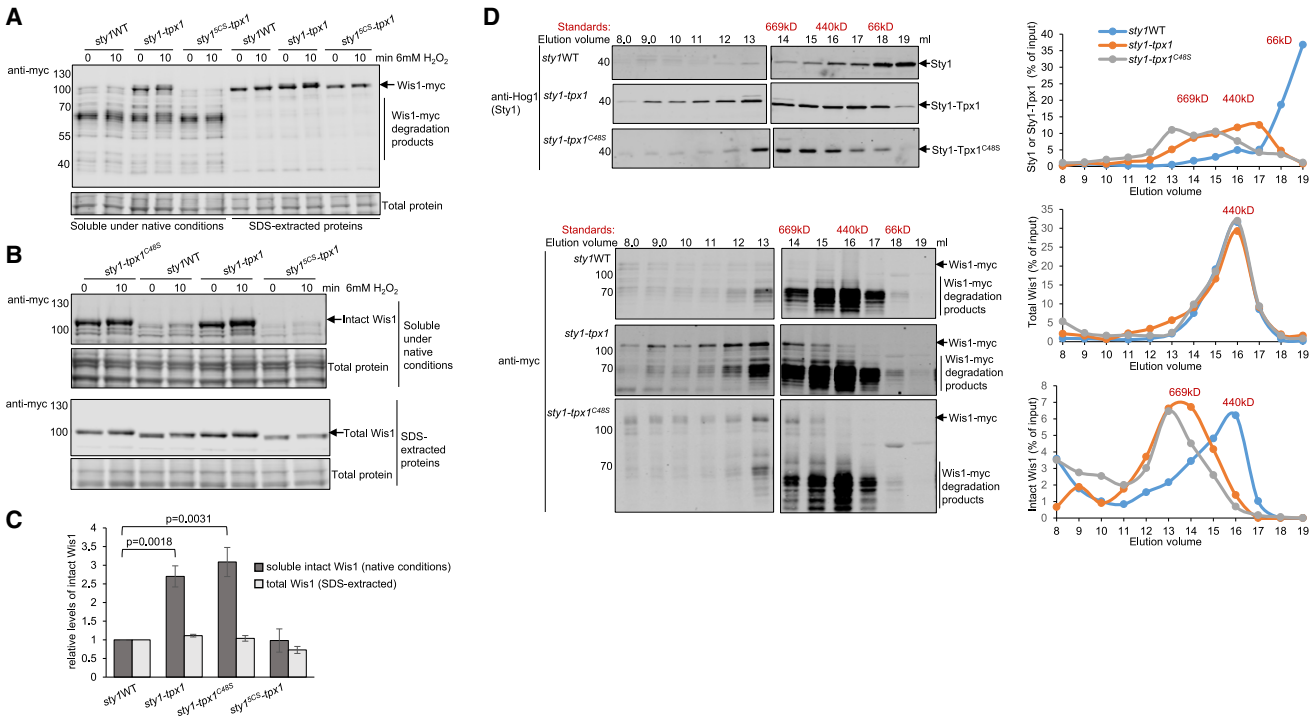

Figure 6. Sty1-Tpx1 complexes promote the assembly of Wis1 into large complexes that protect Wis1 from post-lysis degradation

(A–C) Immunoblot analysis comparing soluble proteins extracted under native (non-denaturing) conditions with SDS-extracted whole-cell extracts from cells co-expressing myc-tagged Wis1 with *sty1WT* (MC2), *sty1-tpx1* (MC12), sty1-tpx1^{C48S} (MC82), or *sty^{5CS}-tpx1* (MC13). Cells were harvested before and after treatment for 10 min with 6 mM H_2O_2 and Wis1 detected using anti-myc antibodies.

(C) The mean level of intact Wis1 (band mobility ~100 kDa) ± SEM relative to Sty1*WT* (MC2) as determined from 3–9 biological repeats indicates that, although total Wis1 levels (SDS-extracted) are similar, the levels of intact Wis1 in extracts prepared under native conditions were ~3× higher in cells expressing Sty1-Tpx1 (MC12) (t test p = 0.0018) or Sty1-Tpx1^{C48S} (MC82) (t test p = 0.0010) fusion proteins compared with wild-type Sty1 (MC2). Levels of Wis1 expression (SDS-extracted) may be lower in Sty1^{5CS}-Tpx1 (MC13) than in wild-type cells (t test = 0.064).

(D) Immunoblot analysis of Sty1 (anti-Hog1) and Wis1 (anti-myc) in eluted fractions from size exclusion chromatography (Superose 6) separation of native protein extracts from cells expressing wild-type Sty1 (MC2), Sty1-Tpx1 (MC12), or Sty1-Tpx1^{C48S} (MC13) fusion proteins. Graphs show the quantification of Sty1 or Wis1 protein levels in each fraction relative to the levels in a 0.4% input lane on the same gel. "Total Wis1" quantification includes the signal from the degradation products. "Intact Wis1" includes only the band ~100 kDa indicated by arrows. The elution volume of standard proteins of known molecular weights is indicated above immunoblots and graphs.

sufficient to increase Wis1/Sty1 activity and accelerate entry into mitosis, even in the absence of Mcs4.

Sty1-Tpx1 complexes provide a "protective" scaffold for Wis1

Our data suggested that Sty1-Tpx1 complexes provide a scaffold that promotes activation of Wis1 by phosphorylation, increasing Sty1 activity and accelerating entry into mitosis (Figure 5C). To explore this model further, we set out to examine how Sty1-Tpx1 complexes affected interactions with Wis1. Intriguingly, this revealed that in cell extracts prepared under native (non-denaturing) conditions, Wis1 was extremely sensitive to cleavage and partial degradation (Figure 6A). Strikingly, although Sty1-Tpx1 and wild-type cells express similar levels of Wis1 (Figures 3, 4, and 6), much greater levels of intact Wis1 were present in native protein extracts prepared from Sty1-Tpx1 fusion-expressing cells (Figures 6A–6C). It was possible this increased resistance to post-lysis degradation reflected the increased Wis1 phosphorylation in cells expressing the Sty1-Tpx1 fusion protein. However, even when wild-type cells were exposed to sufficient H_2O_2 to induce maximal Wis1 phosphorylation (Figure 3A), levels of intact Wis1 present in native protein extracts were much lower than in extract from cells expressing Sty1-Tpx1 fusion proteins (Figures 6A and 6B). This strongly suggested that Sty1-Tpx1 complexes, rather than phosphorylation, protect Wis1 in native extracts from post-lysis proteolytic degradation. Significantly, analysis of Sty1-Tpx1^{C48S}-expressing cells demonstrated that the peroxide-reacting cysteine of Tpx1 was dispensable for protecting Wis1 from post-lysis degradation (Figures 6B and 6C).

Next, we explored the basis for this protective effect on Wis1. An important function of scaffold proteins is to support interactions between signaling proteins, including promoting their assembly into high molecular weight complexes that are a feature of activated P38 signaling.[52,53] Hence, we investigated whether the expression of Sty1-Tpx1 impacted the size of complexes involving Sty1 and/or Wis1. To do this, we fractionated native cell lysate from cells expressing wild-type Sty1 or Sty1-Tpx1 fusion proteins using size exclusion chromatography on

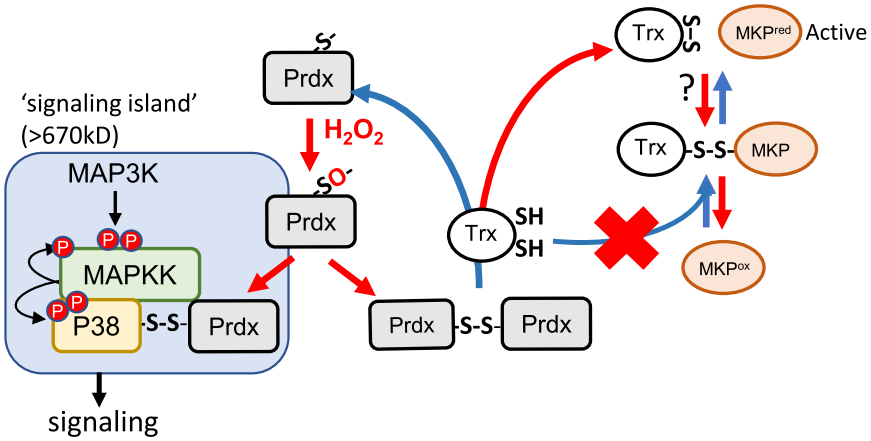

Figure 7. Model, based on our work in yeast, illustrating how Prdx-disulfide complexes and thioredoxin peroxidase activity mediate H_2O_2 signal transduction to P38 MAPK pathways

Based on our work in yeast, we propose that Prdx (Tpx1) can act as a peroxide transducer to increase activation of the P38 MAPK (Sty1) in fission yeast by two independent mechanisms: first, (as depicted on the right-hand side) the reduction of Prdx-Prdx disulfides promotes oxidation of thioredoxin (Trx)[20] and, accordingly, the oxidation of the MAPK phosphatase (MKP) Pyp1, inhibiting Pyp1's activity toward Sty1. Thioredoxin reduces disulfide bonds in oxidized proteins, with Trx-MKP disulfide complexes, as illustrated, an expected intermediate in the reduction of MKP. However, our data in Δ*trx1* mutant cells (Figure 2) are consistent with oxidized Trx1 accepting electrons from reduced Pyp1 (as indicated "?"). Second, (as depicted on the left-hand side) Prdx-P38 MAPK complexes stabilize interactions with the MAPKK (Wis1) to provide a MAPKK-MAPK "signaling island" that allows increased autophosphorylation and canonical autophosphorylation of the MAPKK. In yeast, we show that constitutive Sty1-Tpx1 complex formation drives downstream signaling that accelerated entry into mitosis (Figure 5C). See also Figure S7.

Superose 6 columns, calibrated against protein standards. Immunoblot analysis of the eluted fractions revealed that, although some Sty1 was present in earlier fractions, the majority eluted in later fractions (≤100 kDa), where it was unlikely to be associated with Wis1-myc. By contrast, a significant proportion of Sty1-Tpx1 and Sty1-Tpx1^{C48S} were detected in much earlier fractions consistent with their incorporation into much larger protein complexes (≥440 kDa) (Figure 6D).

Next, we examined how the expression of Sty1-Tpx1 fusion proteins affected the elution profile of Wis1. The peak detection of Wis1 (including Wis1 degradation products) suggested Wis1 was present in complexes ~500 kDa in cells expressing either wild-type Sty1 or Sty1-Tpx1 fusion proteins. However, our analysis indicated that some Wis1 was present in much larger complexes, particularly in cells expressing Sty1-Tpx1 of Sty1-Tpx1^{C48S} fusion proteins (Figure 6D). In contrast to the partial degradation of Wis1 in lower molecular weight complexes, the majority of Wis1 in these large complexes (>670 kDa) was not degraded. Indeed, quantification revealed that the peak of intact Wis1 was shifted from ~440 kDa in wild-type cells to ~700 kDa in cells expressing Sty1-Tpx1 fusions proteins (Figure 6D). The presence of co-eluting Sty1-Tpx1 fusion proteins in these fractions is consistent with Sty1-Tpx1 complexes providing a scaffold and, potentially, protection from proteases, by enhancing interactions between Sty1, Wis1, and other signaling proteins.

In summary, our data suggest that the Prdx Tpx1 facilitates H_2O_2-dependent activation of the Sty1 MAPK by two mechanisms: (1) by promoting thioredoxin-dependent oxidation of the MAPK tyrosine phosphatase Pyp1 and (2) by forming disulfide complexes with Sty1. Our data suggest that Tpx1-Sty1 complexes provide a scaffold stabilizing Wis1/Sty1 interactions, thus supporting the canonical and non-canonical autophosphorylation of the MAPKK Wis1 and driving cells into mitosis (Figures 7 and 5C). We suggest that these two mechanisms confer H_2O_2-sensitivity on the P38 pathway, facilitating the activation of Sty1 by H_2O_2 levels far below the threshold for activating the canonical MAP3K (Figures 7 and S7).

DISCUSSION

Here, we demonstrate that the formation of a complex with a Prdx can be sufficient to increase the activity of P38 MAPK. Our data suggest the Prdx-MAPK complex in fission yeast provides a scaffold supporting the increased activation of the corresponding MAPKK via both canonical MAP3K and non-canonical autophosphorylation mechanisms. Using cells engineered to express P38-Prdx fusions, we show that complexes between Prdx and P38α MAPK can also increase the phosphorylation of human P38, suggesting this peroxidase-independent function for Prdx in activating P38 MAPK is conserved in other eukaryotes.

It will be interesting to determine whether the two domains of the Prdx-MAPK fusion protein interact and/or whether the scaffold function depends on interactions between Prdx subunits, which readily oligomerize. In this regard, this scaffold function is reminiscent of the role that the small ubiquitin-like modifier SUMO can play in regulating protein activity and signal transduction.[54,55] Although SUMOylation occurs on specific lysine side-chains, SUMO acts as an independent "domain," modulating the interactions of signaling proteins regardless of where it is covalently linked to its target protein.[37] Structurally, Prdx contain a thioredoxin fold and are members of the thioredoxin superfamily. Although the majority of thioredoxin-fold-containing proteins have redox catalytic activities, significantly, redox-inactive thioredoxin domains perform well-established scaffolding/non-redox functions in protein disulfide isomerases. Hence, we speculate that Tpx1 may act in a similar manner to SUMOylation, independently modulating Sty1/Wis1 activity regardless of its position in relation to Sty1.

Notably, many proteins form disulfide-bonded complexes with Prdxs, provoking speculation that these complexes mediate H_2O_2 signaling by post-translationally modifying the activity of the partner protein as shown here for Sty1.[56,57] Our finding that Sty1-Tpx1 complexes promote the assembly of Wis1/Sty1 into larger multiprotein complexes raises the possibility that disulfide complexes with Prdxs may also stabilize the complexes in which other partner proteins participate.

Our data suggest the thioredoxin peroxidase activity of Tpx1 increases Sty1 activation by indirectly promoting the formation of disulfide-bonded complexes involving the MKP Pyp1. Although the molecular nature of the higher-molecular-weight (HMW) disulfide complexes Pyp1 forms is unclear, P38 MKPs are inhibited by oxidation to HMW disulfide complexes in mammalian cells.[58,59] Pyp1 is susceptible to heat stress-induced aggregation, which provides a mechanism for activation of Sty1 by heat stress.[60–62] Redox-regulated protein-protein interactions can also influence the duration of PTP inhibition in other ways.[59–63] For example, PTPs, including the p38α MKP HePTP, are regulated by reversible oxidation of the invariant catalytic cysteine, with the formation of intermolecular disulfide bonds, an established mechanism for preventing irreversible oxidation.[9,64] Thus, we propose that these Prdx/Trx-dependent disulfide complexes allow transient, reversible inactivation of Pyp1 in response to H_2O_2. Notably, thioredoxin is important for H_2O_2-induced activation of Sty1 and the *Candida albicans* P38 MAPK Hog1, suggesting that this phosphatase-regulatory mechanism may be conserved.[65]

Localized increases in endogenous H_2O_2 can initiate physiological responses. Prdxs are directly involved in some of these responses, via disulfide complexes with signaling proteins, as described here for the P38 MAPK Sty1 (and other examples reviewed in Bolduc et al.[2] and Winterbourn[66]). However, we could find no evidence for a direct role for Tpx1 in Pyp1 oxidation. Instead, our data suggest that Prdx-driven localized oxidation of thioredoxin could provide another way to relay H_2O_2 signals to nearby signaling proteins. In the case of Pyp1, our data suggest this occurs via a direct mechanism, potentially involving oxidized thioredoxin-accepting electrons from low redox potential cysteines on Pyp1. However, the Prdx-driven oxidation of thioredoxin will also prevent the thioredoxin-mediated reduction of disulfide bond/s formed by other mechanisms. Consistent with both possible roles for thioredoxin, less Pyp1 oxidation was detected in response to higher concentrations of H_2O_2. Although seemingly counter-intuitive, parallels with the Tpx1-dependent oxidation of Pap1 suggest that this may reflect increased availability of reduced thioredoxin when the thioredoxin peroxidase activity of Tpx1 is inhibited by hyperoxidation of its peroxide-reacting cysteine.[16,18,19,30] By contrast, our experiments suggest that the scaffold function of Tpx1-disulfide complexes contributes to Sty1 activation over a broader range of H_2O_2 concentrations.

In *S. pombe*, the glyceraldehyde phosphate dehydrogenase Tdh1 and two-component signaling proteins regulating Mcs4 are important for increased MAP3K activity in response to H_2O_2.[45,46,48] Unexpectedly, we only detected significant increases in MAP3K activity following exposure to much higher doses of H_2O_2 than those required to activate Sty1. By contrast, both the Tpx1-dependent oxidation of Pyp1 and the formation of Tpx1-Sty1 disulfide complexes occur coincident with the increased phosphorylation of Sty1 in response to lower, sub-lethal levels of H_2O_2. This highlights the key role that Tpx1-dependent oxidation events play in facilitating Sty1-mediated adaptive responses to lower levels of H_2O_2. Moreover, we demonstrate that Tpx1-driven oxidation of Pyp1 and Sty1-Tpx1 complexes act by independent mechanisms, synergistically activating Sty1. This combination of Tpx1-dependent MAPKK activation and inhibition of the MKP Pyp1 provides an attractive mechanism to tailor a rapid response to small increases in H_2O_2 insufficient to activate MAP3K. Intriguingly, it has also been shown that the upstream activators of P38 in mammalian cells (MKK3 and MKK6) can be modulated through intramolecular or intermolecular disulfide signaling to P38, suggesting that aspects of our regulatory framework are conserved.[67,68]

Finally, we reveal that Wis1 undergoes additional stress-induced, non-canonical phosphorylation events that are also stimulated by the presence of Sty1-Tpx1 complexes. Although we have not determined their precise nature, our analysis of cells expressing Wis1 mutants with much lower kinase activity suggests that autophosphorylation is involved. It will be interesting to determine how this autophosphorylation contributes to Wis1 activity. Future investigations will also determine whether the multiprotein complexes to which Wis1/Sty1 are recruited by Sty1-Tpx1 complexes are specifically targeted toward unidentified, pro-mitotic substrates rather than those mediating stress-induced mitotic delay. Given the intense interest in therapeutic targeting of the P38 pathway, we anticipate that these discoveries could suggest new avenues for modulating this signaling node. A major challenge for the clinical use of P38 inhibitors is specifically targeting cells that depend on elevated P38 activity, avoiding the unwanted side effects of broadly inhibiting P38 activity in all cells.[69] Here, we demonstrate that constitutive P38-Prdx complex formation represents a non-canonical mechanism to activate P38 MAPKs, which is lethal when combined with loss of MKP activity. This could invite new strategies to specifically target P38 signaling outputs in tumor cells with elevated Prdx levels or in which P38 is hyperactivated due to the absence of normal feedback mechanisms.

Limitations of the study

We show that, in the absence of an activating stimulus, ectopically expressed Prdx1-P38α and Prdx2-P38α fusion proteins are preferentially phosphorylated on the TGY-activating motif in cells co-expressing endogenous P38. This is consistent with Prdx-P38α complexes providing a scaffold for P38 activation in human cells, as observed in yeast expressing Tpx1-Sty1. Constitutive Tpx1-Sty1 complex formation stabilizes multiprotein complexes involving Wis1, increases phosphorylation of at least one Sty1 substrate, and accelerates entry into mitosis. However, the biological consequence/s of the hyperphosphorylation of P38α-Prdx complexes for the regulation of downstream substrates remains to be determined. It is possible that P38α-Prdx and Tpx1-Sty1 complex formation directs P38/Sty1 activity toward a subset/s of known or unknown substrates, potentially in specific complexes or cell compartment/s. Further studies to elucidate the *in vivo* targets of Prdx-P38 fusion proteins will be required to test this hypothesis.

STAR★METHODS

Detailed methods are provided in the online version of this paper and include the following:

- KEY RESOURCES TABLE
- RESOURCE AVAILABILITY
  - Lead contact
  - Materials availability
  - Data and code availability

SUPPLEMENTAL INFORMATION

Supplemental information can be found online at https://doi.org/10.1016/j.molcel.2023.07.018.

ACKNOWLEDGMENTS

We thank Professors Janni Petersen, Janet Quinn, Ken Sawin, Per Sunnerhagen, and Dr. Johanna Sjölander for kindly sharing *S. pombe* strains and Professor Janet Quinn, Dr. Josana Rodriguez, and Dr. Paraskevi Kritsiligkou for valuable manuscript discussions. We thank the BBSRC for funding BB/T002484/1 (M.C., E.B., and E.A.V.), BB/F023065/1 (A.M.D. and E.A.V.), BBSRC DTP studentships (BB/M011186/1 to M.G. and E.A.V., BB/J014516/1 to H.R.L. and E.A.V., and BB/T008695/1 to E.D., T.W.F., and E.A.V.). P.A.E. and D.P.B. acknowledge funding from the NIH Illuminating the Druggable Genome (IDG) common fund consortium (NCI U01CA239106), BBSRC grants BB/S018514/1 and BB/N021703/1, and North West Cancer Research (NWCR) grant CR1208.

AUTHOR CONTRIBUTIONS

Conceptualization, E.A.V. and M.G.; methodology, E.A.V., M.G., M.C., D.P.B., P.A.E., J.P., H.R.L., and E.D.; validation, M.C., H.R.L., M.G., D.P.B., and T.W.F.; investigation, M.C., A.M.D., M.G., H.R.L., D.P.B., E.B., T.W.F., and J.P.; writing – original draft, E.A.V., M.C., M.G., A.M.D., D.P.B., and P.A.E.; writing – review & editing, E.A.V., M.C., M.G., A.M.D., D.P.B., P.A.E., and B.A.M.; supervision, E.A.V. and P.A.E.; project administration, E.A.V.; funding acquisition, E.A.V., B.A.M., and P.A.E.

DECLARATION OF INTERESTS

The authors declare no competing interests.

INCLUSION AND DIVERSITY

We support inclusive, diverse, and equitable conduct of research.

Received: October 24, 2022
Revised: May 19, 2023
Accepted: July 14, 2023
Published: August 11, 2023

REFERENCES

1. Nyström, T., Yang, J., and Molin, M. (2012). Peroxiredoxins, gerontogenes linking aging to genome instability and cancer. Genes Dev. *26*, 2001–2008. 26/18/2001. https://doi.org/10.1101/gad.200006.112.
2. Bolduc, J., Koruza, K., Luo, T., Malo Pueyo, J., Vo, T.N., Ezeriņa, D., and Messens, J. (2021). Peroxiredoxins wear many hats: factors that fashion their peroxide sensing personalities. Redox Biol. *42*, 101959. https://doi.org/10.1016/j.redox.2021.101959.
3. Kowalczyk, K.M., Hartmuth, S., Perera, D., Stansfield, P., and Petersen, J. (2013). Control of Sty1 MAPK activity through stabilisation of the Pyp2 MAPK phosphatase. J. Cell Sci. *126*, 3324–3332. https://doi.org/10.1242/jcs.122531.
4. Holmström, K.M., and Finkel, T. (2014). Cellular mechanisms and physiological consequences of redox-dependent signalling. Nat. Rev. Mol. Cell Biol. *15*, 411–421. https://doi.org/10.1038/nrm3801.
5. Hurd, T.R., DeGennaro, M., and Lehmann, R. (2012). Redox regulation of cell migration and adhesion. Trends Cell Biol. *22*, 107–115. https://doi.org/10.1016/j.tcb.2011.11.002.
6. Veal, E.A., Day, A.M., and Morgan, B.A. (2007). Hydrogen peroxide sensing and signaling. Mol. Cell *26*, 1–14. https://doi.org/10.1016/j.molcel.2007.03.016.
7. Delaunay, A., Pflieger, D., Barrault, M.-B., Vinh, J., and Toledano, M.B. (2002). A thiol peroxidase is an H_2O_2 receptor and redox-transducer in gene activation. Cell *111*, 471–481. https://doi.org/10.1016/s0092-8674(02)01048-6.
8. Dansen, T.B., Smits, L.M.M., van Triest, M.H., de Keizer, P.L.J., van Leenen, D., Koerkamp, M.G., Szypowska, A., Meppelink, A., Brenkman, A.B., Yodoi, J., et al. (2009). Redox-sensitive cysteines bridge p300/CBP-mediated acetylation and FoxO4 activity. Nat. Chem. Biol. *5*, 664–672. https://doi.org/10.1038/nchembio.194.
9. Tonks, N.K. (2005). Redox redux: revisiting PTPs and the control of cell signaling. Cell *121*, 667–670. https://doi.org/10.1016/j.cell.2005.05.016.
10. Byrne, D.P., Shrestha, S., Galler, M., Cao, M., Daly, L.A., Campbell, A.E., Eyers, C.E., Veal, E.A., Kannan, N., and Eyers, P.A. (2020). Aurora A regulation by reversible cysteine oxidation reveals evolutionarily conserved redox control of Ser/Thr protein kinase activity. Sci. Signal. *13*, eaax2713. https://doi.org/10.1126/scisignal.aax2713.
11. Hourihan, J.M., Moronetti Mazzeo, L.E., Fernández-Cárdenas, L.P., and Blackwell, T.K. (2016). Cysteine sulfenylation directs IRE-1 to activate the SKN-1/Nrf2 antioxidant response. Mol. Cell *63*, 553–566. https://doi.org/10.1016/j.molcel.2016.07.019.
12. Wani, R., Qian, J., Yin, L., Bechtold, E., King, S.B., Poole, L.B., Paek, E., Tsang, A.W., and Furdui, C.M. (2011). Isoform-specific regulation of Akt by PDGF-induced reactive oxygen species. Proc. Natl. Acad. Sci. USA *108*, 10550–10555. https://doi.org/10.1073/pnas.1011665108.
13. Winterbourn, C.C. (2008). Reconciling the chemistry and biology of reactive oxygen species. Nat. Chem. Biol. *4*, 278–286. https://doi.org/10.1038/nchembio.85.
14. Okazaki, S., Naganuma, A., and Kuge, S. (2005). Peroxiredoxin-mediated redox regulation of the nuclear localization of Yap1, a transcription factor in budding yeast. Antioxid. Redox Signal. *7*, 327–334. https://doi.org/10.1089/ars.2005.7.327.
15. Sobotta, M.C., Liou, W., Stöcker, S., Talwar, D., Oehler, M., Ruppert, T., Scharf, A.N.D., and Dick, T.P. (2015). Peroxiredoxin-2 and STAT3 form a redox relay for H_2O_2 signaling. Nat. Chem. Biol. *11*, 64–70. https://doi.org/10.1038/nchembio.1695.
16. Bersweiler, A., D'Autréaux, B., Mazon, H., Kriznik, A., Belli, G., Delaunay-Moisan, A., Toledano, M.B., and Rahuel-Clermont, S. (2017). A scaffold protein that chaperones a cysteine-sulfenic acid in H2O2 signaling. Nat. Chem. Biol. *13*, 909–915. https://doi.org/10.1038/nchembio.2412.
17. Bozonet, S.M., Findlay, V.J., Day, A.M., Cameron, J., Veal, E.A., and Morgan, B.A. (2005). Oxidation of a eukaryotic 2-Cys peroxiredoxin is a

molecular switch controlling the transcriptional response to increasing levels of hydrogen peroxide. J. Biol. Chem. *280*, 23319–23327. https://doi.org/10.1074/jbc.M502757200.

18. Brown, J.D., Day, A.M., Taylor, S.R., Tomalin, L.E., Morgan, B.A., and Veal, E.A. (2013). A peroxiredoxin promotes H2O2 signaling and oxidative stress resistance by oxidizing a thioredoxin family protein. Cell Rep. *5*, 1425–1435. https://doi.org/10.1016/j.celrep.2013.10.036.
19. Vivancos, A.P., Castillo, E.A., Biteau, B., Nicot, C., Ayté, J., Toledano, M.B., and Hidalgo, E. (2005). A cysteine-sulfinic acid in peroxiredoxin regulates H2O2-sensing by the antioxidant Pap1 pathway. Proc. Natl. Acad. Sci. USA *102*, 8875–8880. https://doi.org/10.1073/pnas.0503251102.
20. Day, A.M., Brown, J.D., Taylor, S.R., Rand, J.D., Morgan, B.A., and Veal, E.A. (2012). Inactivation of a peroxiredoxin by hydrogen peroxide is critical for thioredoxin-mediated repair of oxidized proteins and cell survival. Mol. Cell *45*, 398–408. https://doi.org/10.1016/j.molcel.2011.11.027.
21. Bodvard, K., Peeters, K., Roger, F., Romanov, N., Igbaria, A., Welkenhuysen, N., Palais, G., Reiter, W., Toledano, M.B., Käll, M., and Molin, M. (2017). Light-sensing via hydrogen peroxide and a peroxiredoxin. Nat. Commun. *8*, 14791. https://doi.org/10.1038/ncomms14791.
22. Dangoor, I., Peled-Zehavi, H., Wittenberg, G., and Danon, A. (2012). A chloroplast light-regulated oxidative sensor for moderate light intensity in *Arabidopsis*. Plant Cell *24*, 1894–1906. https://doi.org/10.1105/tpc.112.097139.
23. Ojeda, V., Pérez-Ruiz, J.M., and Cejudo, F.J. (2018). The NADPH-dependent thioredoxin reductase C-2-Cys peroxiredoxin redox system modulates the activity of thioredoxin x in Arabidopsis chloroplasts. Plant Cell Physiol. *59*, 2155–2164. https://doi.org/10.1093/pcp/pcy134.
24. Canovas, B., and Nebreda, A.R. (2021). Diversity and versatility of p38 kinase signalling in health and disease. Nat. Rev. Mol. Cell Biol. *22*, 346–366. https://doi.org/10.1038/s41580-020-00322-w.
25. Cuenda, A., and Rousseau, S. (2007). p38 MAP-Kinases pathway regulation, function and role in human diseases. Biochim. Biophys. Acta *1773*, 1358–1375. https://doi.org/10.1016/j.bbamcr.2007.03.010.
26. Johnson, G.L., and Lapadat, R. (2002). Mitogen-activated protein kinase pathways mediated by ERK, JNK, and p38 protein kinases. Science *298*, 1911–1912. https://doi.org/10.1126/science.1072682.
27. Sanz-Ezquerro, J.J., and Cuenda, A. (2021). p38 signalling pathway. Int. J. Mol. Sci. *22*, 1003. https://doi.org/10.3390/ijms22031003.
28. Millar, J.B., Buck, V., and Wilkinson, M.G. (1995). Pyp1 and Pyp2 PTPases dephosphorylate an osmosensing MAP kinase controlling cell size at division in fission yeast. Genes Dev. *9*, 2117–2130. https://doi.org/10.1101/gad.9.17.2117.
29. Shiozaki, K., and Russell, P. (1995). Cell-cycle control linked to extracellular environment by MAP kinase pathway in fission yeast. Nature *378*, 739–743. https://doi.org/10.1038/378739a0.
30. Degols, G., Shiozaki, K., and Russell, P. (1996). Activation and regulation of the Spc1 stress-activated protein kinase in *Schizosaccharomyces pombe*. Mol. Cell. Biol. *16*, 2870–2877. https://doi.org/10.1128/mcb.16.6.2870.
31. Veal, E.A., Findlay, V.J., Day, A.M., Bozonet, S.M., Evans, J.M., Quinn, J., and Morgan, B.A. (2004). A 2-Cys peroxiredoxin regulates peroxide-induced oxidation and activation of a stress-activated MAP kinase. Mol. Cell *15*, 129–139. https://doi.org/10.1016/j.molcel.2004.06.021.
32. Barata, A.G., and Dick, T.P. (2020). A role for peroxiredoxins in H2O2- and MEKK-dependent activation of the p38 signaling pathway. Redox Biol. *28*, 101340. https://doi.org/10.1016/j.redox.2019.101340.
33. Conway, J.P., and Kinter, M. (2006). Dual role of peroxiredoxin I in macrophage-derived foam cells. J. Biol. Chem. *281*, 27991–28001. https://doi.org/10.1074/jbc.M605026200.
34. De Haes, W., Frooninckx, L., Van Assche, R., Smolders, A., Depuydt, G., Billen, J., Braeckman, B.P., Schoofs, L., and Temmerman, L. (2014). Metformin promotes lifespan through mitohormesis via the peroxiredoxin PRDX-2. Proc. Natl. Acad. Sci. USA *111*. E2501–E2509. https://doi.org/10.1073/pnas.1321776111.
35. Jarvis, R.M., Hughes, S.M., and Ledgerwood, E.C. (2012). Peroxiredoxin 1 functions as a signal peroxidase to receive, transduce, and transmit peroxide signals in mammalian cells. Free Radic. Biol. Med. *53*, 1522–1530. https://doi.org/10.1016/j.freeradbiomed.2012.08.001.
36. Oláhová, M., Taylor, S.R., Khazaipoul, S., Wang, J., Morgan, B.A., Matsumoto, K., Blackwell, T.K., and Veal, E.A. (2008). A redox-sensitive peroxiredoxin that is important for longevity has tissue- and stress-specific roles in stress resistance. Proc. Natl. Acad. Sci. USA *105*, 19839–19844. https://doi.org/10.1073/pnas.0805507105.
37. Ross, S., Best, J.L., Zon, L.I., and Gill, G. (2002). SUMO-1 modification represses Sp3 transcriptional activation and modulates its subnuclear localization. Mol. Cell *10*, 831–842. https://doi.org/10.1016/s1097-2765(02)00682-2.
38. Smith, F.D., Esseltine, J.L., Nygren, P.J., Veesler, D., Byrne, D.P., Vonderach, M., Strashnov, I., Eyers, C.E., Eyers, P.A., Langeberg, L.K., and Scott, J.D. (2017). Local protein kinase A action proceeds through intact holoenzymes. Science *356*, 1288–1293. https://doi.org/10.1126/science.aaj1669.
39. Day, A.M., and Veal, E.A. (2010). Hydrogen peroxide-sensitive cysteines in the Sty1 MAPK regulate the transcriptional response to oxidative stress. J. Biol. Chem. *285*, 7505–7516. https://doi.org/10.1074/jbc.M109.040840.
40. Madrid, M., Núñez, A., Soto, T., Vicente-Soler, J., Gacto, M., and Cansado, J. (2007). Stress-activated protein kinase-mediated down-regulation of the cell integrity pathway mitogen-activated protein kinase Pmk1p by protein phosphatases. Mol. Biol. Cell *18*, 4405–4419. https://doi.org/10.1091/mbc.e07-05-0484.
41. Sjölander, J.J., Tarczykowska, A., Picazo, C., Cossio, I., Redwan, I.N., Gao, C., Solano, C., Toledano, M.B., Grøtli, M., Molin, M., and Sunnerhagen, P. (2020). A redox-sensitive thiol in Wis1 modulates the fission yeast mitogen-activated protein kinase response to H2O2 and is the target of a small molecule. Mol. Cell. Biol. *40*, e00346-19. https://doi.org/10.1128/MCB.00346-19.
42. Dagnell, M., Frijhoff, J., Pader, I., Augsten, M., Boivin, B., Xu, J., Mandal, P.K., Tonks, N.K., Hellberg, C., Conrad, M., et al. (2013). Selective activation of oxidized PTP1B by the thioredoxin system modulates PDGF-beta receptor tyrosine kinase signaling. Proc. Natl. Acad. Sci. USA *110*, 13398–13403. https://doi.org/10.1073/pnas.1302891110.
43. Schwertassek, U., Haque, A., Krishnan, N., Greiner, R., Weingarten, L., Dick, T.P., and Tonks, N.K. (2014). Reactivation of oxidized PTP1B and PTEN by thioredoxin 1. FEBS J. *281*, 3545–3558. https://doi.org/10.1111/febs.12898.
44. Machado, L.E.S.F., Shen, T.-L., Page, R., and Peti, W. (2017). The KIM-family protein-tyrosine phosphatases use distinct reversible oxidation intermediates: intramolecular or intermolecular disulfide bond formation. J. Biol. Chem. *292*, 8786–8796. https://doi.org/10.1074/jbc.M116.774174.
45. Buck, V., Quinn, J., Soto Pino, T., Martin, H., Saldanha, J., Makino, K., Morgan, B.A., and Millar, J.B. (2001). Peroxide sensors for the fission yeast stress-activated mitogen-activated protein kinase pathway. Mol. Biol. Cell *12*, 407–419. https://doi.org/10.1091/mbc.12.2.407.
46. Morigasaki, S., Shimada, K., Ikner, A., Yanagida, M., and Shiozaki, K. (2008). Glycolytic enzyme GAPDH promotes peroxide stress signaling through multistep phosphorelay to a MAPK cascade. Mol. Cell *30*, 108–113. https://doi.org/10.1016/j.molcel.2008.01.017.
47. Morigasaki, S., and Shiozaki, K. (2013). Phosphorelay-dependent and -independent regulation of MAPKKK by the Mcs4 response regulator in fission yeast. Commun. Integr. Biol. *6*, e25020. https://doi.org/10.4161/cib.25020.
48. Shiozaki, K., Shiozaki, M., and Russell, P. (1997). Mcs4 mitotic catastrophe suppressor regulates the fission yeast cell cycle through the Wik1-Wis1-Spc1 kinase cascade. Mol. Biol. Cell *8*, 409–419. https://doi.org/10.1091/mbc.8.3.409.

49. Mutavchiev, D.R., Leda, M., and Sawin, K.E. (2016). Remodeling of the fission yeast Cdc42 cell-polarity module via the Sty1 p38 stress-activated protein kinase pathway. Curr. Biol. *26*, 2921–2928. https://doi.org/10.1016/j.cub.2016.08.048.

50. Shiozaki, K., Shiozaki, M., and Russell, P. (1998). Heat stress activates fission yeast Spc1/Styl MAPK by a MEKK-independent mechanism. Mol. Biol. Cell *9*, 1339–1349. https://doi.org/10.1091/mbc.9.6.1339.

51. Gregan, J., Zhang, C., Rumpf, C., Cipak, L., Li, Z., Uluocak, P., Nasmyth, K., and Shokat, K.M. (2007). Construction of conditional analog-sensitive kinase alleles in the fission yeast *Schizosaccharomyces pombe*. Nat. Protoc. *2*, 2996–3000. https://doi.org/10.1038/nprot.2007.447.

52. Good, M.C., Zalatan, J.G., and Lim, W.A. (2011). Scaffold proteins: hubs for controlling the flow of cellular information. Science *332*, 680–686. https://doi.org/10.1126/science.1198701.

53. Bequette, C.J., Hind, S.R., Pulliam, S., Higgins, R., and Stratmann, J.W. (2018). MAP kinases associate with high molecular weight multiprotein complexes. J. Exp. Bot. *69*, 643–654. https://doi.org/10.1093/jxb/erx424.

54. Pelisch, F., Tammsalu, T., Wang, B., Jaffray, E.G., Gartner, A., and Hay, R.T. (2017). A SUMO-dependent protein network regulates chromosome congression during oocyte meiosis. Mol. Cell *65*, 66–77. https://doi.org/10.1016/j.molcel.2016.11.001.

55. Verhelst, K., Carpentier, I., and Beyaert, R. (2011). Regulation of TNF-induced NF- κB activation by different cytoplasmic ubiquitination events. Cytokine Growth Factor Rev. *22*, 277–286. https://doi.org/10.1016/j.cytogfr.2011.11.002.

56. Stöcker, S., Maurer, M., Ruppert, T., and Dick, T.P. (2018). A role for 2-Cys peroxiredoxins in facilitating cytosolic protein thiol oxidation. Nat. Chem. Biol. *14*, 148–155. https://doi.org/10.1038/nchembio.2536.

57. van Dam, L., Pagès-Gallego, M., Polderman, P.E., van Es, R.M., Burgering, B.M.T., Vos, H.R., and Dansen, T.B. (2021). The Human 2-Cys peroxiredoxins form Widespread, cysteine-Dependent- and isoform-Specific protein-protein Interactions. Antioxidants (Basel) *10*, 627. https://doi.org/10.3390/antiox10040627.

58. Kamata, H., Honda, S., Maeda, S., Chang, L., Hirata, H., and Karin, M. (2005). Reactive oxygen species promote TNFα-induced death and sustained JNK activation by inhibiting MAP kinase phosphatases. Cell *120*, 649–661. https://doi.org/10.1016/j.cell.2004.12.041.

59. Turner-Ivey, B., Manevich, Y., Schulte, J., Kistner-Griffin, E., Jezierska-Drutel, A., Liu, Y., and Neumann, C.A. (2013). Role for Prdx1 as a specific sensor in redox-regulated senescence in breast cancer. Oncogene *32*, 5302–5314. https://doi.org/10.1038/onc.2012.624.

60. Nguyen, A.N., and Shiozaki, K. (1999). Heat-shock-induced activation of stress MAP kinase is regulated by threonine- and tyrosine-specific phosphatases. Genes Dev. *13*, 1653–1663. https://doi.org/10.1101/gad.13.13.1653.

61. Samejima, I., Mackie, S., and Fantes, P.A. (1997). Multiple modes of activation of the stress-responsive MAP kinase pathway in fission yeast. EMBO J. *16*, 6162–6170. https://doi.org/10.1093/emboj/16.20.6162.

62. Boronat, S., Marte, L., Vega, M., García-Santamarina, S., Cabrera, M., Ayté, J., and Hidalgo, E. (2020). The Hsp40 Mas5 connects protein quality control and the General Stress response through the thermo-sensitive Pyp1. iScience *23*, 101725. https://doi.org/10.1016/j.isci.2020.101725.

63. Londhe, A.D., Bergeron, A., Curley, S.M., Zhang, F., Rivera, K.D., Kannan, A., Coulis, G., Rizvi, S.H.M., Kim, S.J., Pappin, D.J., et al. (2020). Regulation of PTP1B activation through disruption of redox-complex formation. Nat. Chem. Biol. *16*, 122–125. https://doi.org/10.1038/s41589-019-0433-0.

64. Netto, L.E.S., and Machado, L.E.S.F. (2022). Preferential redox regulation of cysteine-based protein tyrosine phosphatases: structural and biochemical diversity. FEBS J. *289*, 5480–5504. https://doi.org/10.1111/febs.16466.

65. da Silva Dantas, A., Patterson, M.J., Smith, D.A., Maccallum, D.M., Erwig, L.P., Morgan, B.A., and Quinn, J. (2010). Thioredoxin regulates multiple hydrogen peroxide-induced signaling pathways in Candida albicans. Mol. Cell. Biol. *30*, 4550–4563. https://doi.org/10.1128/MCB.00313-10.

66. Winterbourn, C.C. (2020). Hydrogen peroxide reactivity and specificity in thiol-based cell signalling. Biochem. Soc. Trans. *48*, 745–754. https://doi.org/10.1042/BST20190049.

67. Bassi, R., Burgoyne, J.R., DeNicola, G.F., Rudyk, O., DeSantis, V., Charles, R.L., Eaton, P., and Marber, M.S. (2017). Redox-dependent dimerization of p38α mitogen-activated protein kinase with mitogen-activated protein kinase kinase 3. J. Biol. Chem. *292*, 16161–16173. https://doi.org/10.1074/jbc.M117.785410.

68. Diao, Y., Liu, W., Wong, C.C.L., Wang, X., Lee, K., Cheung, P.-y., Pan, L., Xu, T., Han, J., Yates, J.R., III, et al. (2010). Oxidation-induced intramolecular disulfide bond inactivates mitogen-activated protein kinase kinase 6 by inhibiting ATP binding. Proc. Natl. Acad. Sci. USA *107*, 20974–20979. https://doi.org/10.1073/pnas.1007225107.

69. Martínez-Limón, A., Joaquin, M., Caballero, M., Posas, F., and de Nadal, E. (2020). The p38 pathway: from biology to cancer therapy. Int. J. Mol. Sci. *21*, 1913. https://doi.org/10.3390/ijms21061913.

70. Moreno, S., Klar, A., and Nurse, P. (1991). Molecular genetic analysis of fission yeast *Schizosaccharomyces pombe*. Methods Enzymol. *194*, 795–823. https://doi.org/10.1016/0076-6879(91)94059-l.

71. Veal, E.A., Toone, W.M., Jones, N., and Morgan, B.A. (2002). Distinct roles for glutathione S-transferases in the oxidative stress response in Schizosaccharomyces pombe. J. Biol. Chem. *277*, 35523–35531. https://doi.org/10.1074/jbc.M111548200.

72. Delaunay, A., Isnard, A.D., and Toledano, M.B. (2000). H2O2 sensing through oxidation of the Yap1 transcription factor. EMBO J. *19*, 5157–5166. https://doi.org/10.1093/emboj/19.19.5157.

CellPress
OPEN ACCESS

STAR★METHODS

KEY RESOURCES TABLE

REAGENT or RESOURCE	SOURCE	IDENTIFIER
Antibodies		
anti-Myc mouse monoclonal (9E10)	Santa Cruz Biotechnology	Cat##Sc-40; RRID: AB_627268
anti-HA mouse monoclonal (HA-7)	Sigma-Aldrich	Cat#H9658; RRID: AB_260092
anti-FLAG mouse monoclonal	Sigma-Aldrich	Cat#F3165; RRID: AB_259529
anti-Pk (V5 Tag) mouse monoclonal	Sigma-Aldrich	Cat#V8012; RRID: AB_261888
anti-phospho-P38 (Thr180/Tyr182) rabbit polyclonal	Cell signalling	Cat#9211S; RRID: AB_331641
anti-GAPDH rabbit mAb	Cell signalling	Cat#5174S; RRID: AB_10622025
anti-Hog1 rabbit polyclonal antibodies (Y-215)	Santa Cruz Biotechnology	Cat#Sc-9079; RRID: AB_650117
anti-Sty1 rabbit polyclonal antibodies	Eurogentec	Day and Veal[39]
IRDye 680 RD anti-rabbit IgG	LI-COR	Cat#926-68071; RRID: AB_10956166
IRDye 800 CW anti-rabbit IgG	LI-COR	Cat#925-32211; RRID: AB_2651127
IRDye 680 RD anti-mouse IgG	LI-COR	Cat#926-68070; RRID: AB_10956588
IRDye 800 CW anti-mouse IgG	LI-COR	Cat#926-32210; RRID: AB_621842
Anti-mouse IgG (whole molecule)-peroxidase	Sigma-Aldrich	Cat#A4416; RRID: AB_2558167
Anti-rabbit IgG (whole molecule)-peroxidase	Sigma-Aldrich	Cat#A6154; RRID: AB_258284
Bacterial and virus strains		
E. coli	lab strain	DH5α
Chemicals, peptides, and recombinant proteins		
3-BrB-PP1	Abcam	Cat#ab143756
Fluorescent Brightener (Calcofluor)	Sigma-Aldrich	Cat#F3545-5G
Vectashield™ containing 4, 6-diamidino-2-phenylindole (DAPI)	Vector laboratory	Cat#H-1200
Phos-tag™ Acrylamide	NARD Institute, Japan	Cat#AAL-107
5-FAM-IPTSPITTTYFFFKKK-COOH	Pepceuticals	Custom made
N-Ethylmaleimide (NEM)	Sigma-Aldrich	Cat#E3876-5G
4′-acetamido-4′-maleimidylstilbene-2, 2′-disulfonic acid (AMS)	Invitrogen	Cat#A-484
Pierce BCA protien assay kit	Thermo Scientific	Cat#23227
Coomassie protein assay reagent	Sigma-Aldrich	Cat#1856209
Alkaline phosphatase	Roche	Cat#10713023001
Revert 700 total protein stain	LI-COR	Cat#926-11021
Revert Destaining solution	LI-COR	Cat#926-11013
Pierce ECL Plus western blotting substrate	Thermo Scientific	Cat#32132
Deposited data		
Original digital images for Figures	Mendeley	https://doi.org/10.17632/7ymnbnskhy.1
Experimental models: Organisms/strains		
S. pombe: AD21: *h⁻ ade6 his7-366 leu1-32 ura4-D18 tpx1::ura4⁺ sty1-3pk:ura4⁺*	This study (Dissected spores from EV45 x AD13)	AD21
S. pombe: AD38: *h⁻ ade6-M216 his7-366 leu1-32 ura4-D18 sty1::his7⁺ sty1⁺:ura4⁺*	Dr Elizabeth Veal -Reference #38	AD38
S. pombe: AD84: *h⁻ ade6-M216 his7-366 leu1-32 ura4-D18 sty1::his7⁺ sty1^{C13SC35SC153SC158SC242S}:ura4⁺*	This study (pRip42Sty1^{C13SC35SC153SC158SC242S} linearised with BglII and integrated into AD22)	AD84

(*Continued on next page*)

Continued

REAGENT or RESOURCE	SOURCE	IDENTIFIER
S. pombe: AD130: *h? ade6 his7-366 leu1-32 ura4-D18 trx1::kan*^{MX4} *pyp1-3pk:kan* ^{MX6}	This study (Dissected spores from JB30 x AD142)	AD130
S. pombe: AD142: *h*$^{+}$ *ade6 his7-366 leu1-32 ura4-D18 pyp1-3pk:kan*^{MX6}	This study (NJ197 x CHP429)	AD142
S. pombe: AD143: *h? ade6 leu1-32 ura4-D18 pyp1-3pk:kan* ^{MX6} *tpx1::ura4*$^{+}$	This study (AD142 x VX00)	AD143
S. pombe: AD144: *h? ade6 his7-366 leu1-32 ura4-D18 Flag-trx1:ura4*$^{+}$ *trx1::kan*^{MX4} *pyp1-3pk:kan*^{MX6}	This study (Dissected from JB35 x AD142)	AD144
S. pombe: CHP429: *h*$^{-}$ *ade6-M216 his7-366 leu1-32 ura4-D18*	Lab stock	CH429
S. pombe: EB15: *h? ade6 his7-366 leu1-32 ura4-D18 leu1: nmt81:pyp2-13myc:ura4*$^{+}$ *pyp2::kan*^{MX6} *sty1::his7*$^{+}$ *sty1*$^{+}$*:ura4*$^{+}$	This study: (Dissected from JP378 x AD38)	EB15
S. pombe: EB16: *h? leu1: nmt81:pyp2-13myc:ura4*$^{+}$ *pyp2::kan* ^{MX6} *sty1::his7*$^{+}$ *sty1-tpx1*^{C48S}*:ura4*$^{+}$	This study: (Dissected from JP378 x MG18)	EB16
S. pombe: HL2: *h*$^{+}$ *ade6-M216 leu1-32 ura4-D18 pyp1-3pk:ura4*$^{+}$	This study (pRip42pyp1-3pk linearised and integrated into NT4)	HL2
S. pombe: JM1160: *h*$^{+}$ *ade6 his7-366 leu1–32 ura4-D18 sty1::ura4*$^{+}$	Millar et al.[28] (Gift of Dr Millar)	JM1160
S. pombe: KS8226: *h*$^{+}$ *leu1-32 ura4-D18 sty1*^{T97A} *wis1*^{DD}*-12myc:ura4*$^{+}$ *pyp1::ura4*$^{+}$ *pyp2::LEU2 ars1(*BlpI*):Padh13:CRIB-3xmCitrine:LEU2*	Mutavchiev et al.[49] (Gift of Dr Sawin)	KS8226
S. pombe: KS8311: *h*$^{+}$ *leu1-32 ura4-D18 sty1*^{T97A} *wis1*^{DD}*-12myc:ura4*$^{+}$ *pyp1::ura4*$^{+}$ *pyp2::LEU2 ars1(*BlpI*):Padh13:CRIB-3xmCitrine:LEU2* P*act1:lifeactmCherry::leu1*$^{+}$	Mutavchiev et al.[49] (Gift of Dr Sawin)	KS8311
S. pombe: MC2: *h*$^{-}$ *ade6 his7-366 leu1-32 ura4-D18 pyp1-3pk:kan* ^{MX6} *sty1::his7*$^{+}$ *sty1*$^{+}$*:ura4*$^{+}$ *wis1-12myc:ura4*$^{+}$	This study (Dissected from MC1 x JP148)	MC2
S. pombe: MC12: *h*$^{-}$ *ade6 his7-366 leu1-32 ura4-D18 pyp1-3pk kan* ^{MX6} *sty1::his7*$^{+}$ *sty1-tpx1:ura4*$^{+}$ *wis1-12myc:ura4*$^{+}$	This study (Dissected from MC7 x JP148)	MC12
S. pombe: MC13: *h? ade6 his7-366 leu1-32 ura4-D18 pyp1-3pk:kan* ^{MX6} *sty1:: his7*$^{+}$ *sty1* $^{C13SC35SC153SC158SC242S+}$*:ura4*$^{+}$ *-tpx1: ura4*$^{+}$ *wis1-12myc:ura4*$^{+}$	This study (Dissected from MC9 x JP148)	MC13
S. pombe: MC77: *h? ade6 his7-366 leu1-32 ura4-D18 pyp1-3pk:kan* ^{MX6} *sty1::his7*$^{+}$ *sty1*$^{+}$*: ura4*$^{+}$ *mcs4::his7*$^{+}$ *wis1-12myc:ura4*$^{+}$	This study (Dissected from MC2 x JM1468)	MC77
S. pombe: MC82: *h*$^{+}$ *ade6 his7-366 leu1-32 ura4-D18 pyp1-3pk:kan* ^{MX6} *sty1::his7*$^{+}$ *sty1-tpx1*^{C48S}*:ura4*$^{+}$ *wis1-12myc:ura4*$^{+}$	This study (Dissected from MC69 x JP148)	MC82
S. pombe: MC83: *h? ade6 his7-366 leu1-32 ura4-D18 pyp1-3pk:kan* ^{MX6} *sty1::his7*$^{+}$ *sty1-tpx1:ura4*$^{+}$ *wis1-12myc:ura4*$^{+}$ *mcs4::his7*$^{+}$	This study (Dissected from MC12 x JM1468)	MC83
S. pombe: MC88: *h? ade6 his7-366 leu1-32 ura4-D18 pyp1-3pk:kan1 sty1*$^{+}$ *wis1-12myc: ura4*$^{+}$ *tpx1::nat*^{MX6}	This study (Dissected from ZU12 x MC82)	MC88
S. pombe: MC122: *h? ade6 his7-366 leu1-32 ura4-D18 sty1::his7*$^{+}$ *sty1*$^{+}$*:ura4*$^{+}$*wis1*^{AA}*-12myc:ura4*$^{+}$	This study (Dissected from KS2086 x MC98)	MC122

(*Continued on next page*)

Continued

REAGENT or RESOURCE	SOURCE	IDENTIFIER
S. pombe: MC130: *h? ade6 his7-366 leu1-32 ura4-D18 sty1::his7^{+} sty1-tpx1^{C48S}:ura4^{+} wis1^{AA}-12myc:ura4^{+}*	This study (Dissected from KS2086 x MC100)	MC130
S. pombe: MC132: *h? ade6 his7-366 leu1-32 ura4-D18 sty1::his7^{+} sty1^{+}:ura4^{+} wis1-12myc:ura4^{+}*	This study (Dissected from MC2 x MC98)	MC132
S. pombe: MC135: *h? ade6 his7-366 leu1-32 ura4-D18 sty1::his7^{+} sty1-tpx1^{C48S}:ura4^{+} wis1-12myc:ura4^{+}*	This study (Dissected from MC82 x MG18)	MC135
S. pombe: MC150: *h? ade6 his7-366 leu1-32 ura4-D18 sty1::his7^{+} sty1-tpx1:ura4^{+} pyp1::kan^{MX6}*	This study (Dissected from MG17 x NJ102)	MC150
S. pombe: MG17: *h^{-} ade6-M216 his7-366 leu1-32 ura4-D18 sty1::his7^{+} sty1-tpx1:ura4^{+}*	This study (pRip2Sty1-Tpx1 linearised andintegrated into AD22)	MG17
S. pombe: MG18: *h^{-} ade6-M216 his7-366 leu1-32, ura4-D18 sty1::his7^{+} sty1-tpx1^{C48S}:ura4^{+}*	This study (pRip2Sty1-Tpx1^{C47S} linearised andintegrated into AD22)	MG18
S. pombe: MG23: *h^{-} ade6-M216 his7-366 leu1-32 ura4-D18 sty1::his7^{+} sty1 ^{C13SC35SC153SC158SC242S}-tpx1:ura4^{+}*	This study (pRip2Sty1^{C13SC35SC153SC158SC242S}-Tpx1 linearised and integrated into AD22)	MG23
S. pombe: MG46: *h^{+}ade6-M216 leu1-32 ura4-D18 wis1-3pk:ura4^{+}*	This study (pRip42Wis1pkC linearised and integrated into NT4)	MG46
S. pombe: MG47: *h^{+}ade6-M216 leu1-32 ura4-D18 wis1^{M395A}-3pk:ura4+*	This study (pRip42Wis1^{M395A}pkC linearised and integrated into NT4)	MG47
S. pombe: MG48: *h^{+}ade6-M216 leu1-32 ura4-D18 wis1^{M395G}-3pk:ura4^{+}*	This study (pRip42Wis1^{M395G}pkC linearised and integrated into NT4)	MG48
S. pombe: MG49: *h- ade6 leu1-32 ura4-D18 sty1::his7^{+} sty1-tpx1:ura4^{+} wis1-3pk:ura4^{+}*	This study (Dissected from MG17 x MG46)	MG49
S. pombe: MG50: *h^{-} ade6 leu1-32 ura4-D18 sty1::his7^{+} sty1-tpx1:ura4^{+} wis1^{M395A}-3pk:ura4^{+}*	This study (Dissected from MG17 x MG47)	MG50
S. pombe: MG51: *h^{-} ade6 leu1-32 ura4-D18 sty1::his7^{+} sty1-tpx1:ura4^{+} wis1^{M395G}-3pk:ura4^{+}*	This study (Dissected from MG17 x MG48)	MG51
S. pombe: NJ102: *h^{+} ade6-M210 his7-366 leu1-32 ura4-D18 pyp1::kan^{MX6}*	Gift of Drs Wilkinson and Jones Reference #S16	NJ102
Oligonucleotides		
pst1 sty1 mutant N: CCCAGTCTGCAGCTCAT GAACAACAATAAGGGAGTA	Sigma-Aldrich	N/A
sty1 internal F: GAAGGATCAGGTAACTGG	Sigma-Aldrich	N/A
sty1 Nde1 R: CGCCGCCATATGGGATTGC AGTTCATTATC	Sigma-Aldrich	N/A
wis1_auto_*PstI*_Fwd: TATCTGCAGATGTCTT CTCCAAATAATCAACCC	Sigma-Aldrich	N/A
wis1_auto_*KpnI*_Rev: ATAGGTACCCGCTTCT TTTTTCACCTTTCTCTTTA	Sigma-Aldrich	N/A
wis1_mt395_chk_Fwd: TGGCCTTGAAGGAAA TTAGG	Sigma-Aldrich	N/A
Pk_tag_check_Rev: CAAGCAAAGGGTTAGGA ATACCCAT	Sigma-Aldrich	N/A
Pyp1intcheck: TTTAAGGCCAAATATTCTTAA TAC	Sigma-Aldrich	N/A
Pyp1intcheckB: TCTAAAATACCGAAGTCACC AGAA	Sigma-Aldrich	N/A

(*Continued on next page*)

Continued

REAGENT or RESOURCE	SOURCE	IDENTIFIER
Recombinant DNA		
S. pombe wis1^{+} (wild type) orf DNA	IDT	N/A
S. pombe wis1 orf mutant DNA encoding *wis1*^{M395A}	IDT	N/A
S. pombe wis1 orf mutant DNA encoding *wis1*^{M395A}	IDT	N/A
pRep1	Veal et al.[31]	N/A
pRep1tpx1	Veal et al.[31]	N/A
pRep1tpx1^{C170S}	Veal et al.[31]	N/A
pRep1tpx1^{C48S}	Veal et al.[31]	N/A
pRip42pk	Day et al.[20]	N/A
pcDNA3	Invitrogen	N/A
Software and algorithms		
Image Studio Lite	LI-COR	https://www.licor.com/bio/image-studio-lite/
Axiovision	Zeiss	https://www.micro-shop.zeiss.com/en/us/system/software+axiovision-axiovision+program-axiovision+software/10221/
Typhoon FLA9500	GE healthcare	N/A

RESOURCE AVAILABILITY

Lead contact

Further information and requests for resources and reagents should be directed to and will be fulfilled by the lead contact, Elizabeth A. Veal (e.a.veal@ncl.ac.uk).

Materials availability

Yeast strains and plasmids generated by this study (key resources table and Table S1) are available on request from the lead contact.

Data and code availability

- All blots and microscopy images have been deposited at Mendeley Data and are publicly available as of the date of publication. DOI is listed in the key resources table.
- This paper does not report any original code.
- Any additional information required to re-analyze the data reported in this paper is available from the lead contact upon request.

EXPERIMENTAL MODEL AND STUDY PARTICIPANT DETAILS

Yeast strains, growth conditions, and transformation

The *S. pombe* strains used in this study are shown in the key resources table (strains used in main figure experiments) and/or Table S1 (strains used in supplemental figure experiments or to generate strains used in study). Cells were maintained on Ye5S or Edinburgh minimal medium 2(EMM2) including appropriate supplements.[70] SISA strains were maintained on Ye5S media containing 5μM 3-BrB-PP1(Abcam, ab143756) to prevent lethal activation of sty1 and sequenced to confirm continued presence of Wis1^{DD}-expressing allele.[49] For experiments, cells were grown in liquid culture at 30°C to mid-log phase (OD_{595}=0.3-0.5) with constant aeration at 180rpm in Edinburgh minimal medium 2(EMM2) with appropriate supplements, unless otherwise indicated. DNA was introduced into cells by lithium acetate based chemical transformation.

Mammalian cell growth and transfection

HEK-293T cells were cultured in Dulbecco's modified Eagle medium (Lonza) supplemented with 10% fetal bovine serum (HyClone), penicillin (50 U/ml), and streptomycin (0.25 μg/ml) (Lonza) and maintained at 37°C in 5% CO_2 humidified atmosphere. HEK-293T cells

CellPress
OPEN ACCESS

were transfected using a 3:1 polyethylenimine (PEI [branched average M_w ~25,000 Da; Sigma-Aldrich]) to DNA ratio (30:10 μg, for a single 10-cm culture dish).

METHOD DETAILS

Spot tests to analyze yeast cell growth and adaptation to stress conditions

An equal number of exponentially growing cells were serially diluted 10-fold and spotted on to Ye5S containing 0.4 mM H_2O_2, 1 mM H_2O_2 or 0.5 M KCl. Plates were incubated at 30°C for 2-4 days before imaging.

Plasmid and strain construction

Construction of Sty1-Tpx1 expressing gene fusion strains expressed from S. pombe sty1 locus

pRip2*tpx1*+ and pRip2*tpx1*^{C48S} were generated by removing ARS region from pRep2*tpx1* or pRep2*tpx1*^{C48S} using *EcoRI*.[31] The *sty1*$^{+}$, *sty1*$^{5CS+}$ and *sty1*^{T97A} genes including 1.5kb of the *sty1* promoter up stream of the open reading frames were amplified by Phusion (Thermo Scientific) PCR from NT5, AD84 and KS7830 genomic DNA respectively using primers containing *PstI* and *NdeI* restriction sites at 5' end and 3' end respectively. The amplified PCR products were cloned into *PstI* and *NdeI* sites of pRip2*tpx1*$^{+}$ or pRip2*tpx1*^{C48S}. The recombinant plasmids were linearised with *NheI* and transformed in to AD22. The sequences of sty1 promoter, *sty1*/*sty1*^{5CS}/*sty1*^{T97A} ORF were confirmed by sequencing (Eurofins) of DNA from URA+ transformants using primers *PstI* sty1 mutant N and sty1 internal F.

Construction of S. pombe expressing Pk-tagged Pyp1 from the pyp1 locus

The *pyp1*$^{+}$ orf *was amplified* by PCR using primers containing Pst1 and BamH1 sites and ligated into Pst1/BamHI digested pRip42PkC to create pRip42Pyp2PkC. This was linearised with Sal1 and transformed into wild-type (NT4) cells. URA+ colonies were screened for integration at *pyp1*$^{+}$ locus by colony pcr and sequenced with Pyp1intcheck and Pyp1intcheckB primers.

Construction of S. pombe expressing Pk-tagged Wis1, wis1^{M395A}*, and wis1*^{M395G} *mutant proteins from the wis1 locus*

Mutations of gate-keeper residue Methionine 395 in wis1 ATP-binding pocket were designed to confer sensitivity to small-molecule inhibitors.[51] Wild-type *wis1*$^{+}$ open reading frame or versions in which Methionine at 395 was substituted with alanine or glycine were synthesised by integrated DNA technologies (IDT) with *PstI* site at 5'end and *KpnI* site at 3'end and cloned into pJet1.2 (Thermo Scientific). Wild-type *wis1*$^{+}$ ORF was amplified by Phusion PCR from NT4 genomic DNA with primers containing *PstI* and *KpnI* restriction sites at 5' end and 3' end respectively. Amplified PCR products were digested then ligated into *PstI* and *KpnI* sites of pRip42pk[20] to generate pRip42Wis1pkC, pRip42Wis1^{M395G}pkC or pRip42Wis1^{M395A}pkC. Recombinant plasmids were linearised with *ApaI* and transformed into NT4 strain and URA+ colonies screened by colony pcr for integration at *wis1*$^{+}$ locus with wis1_auto_*PstI*_F and pk_tag_check_rev primers, then sequenced with wis1_mt395_chk_fwd primer.

Construction of P38-PRDX1/2 fusion plasmids for expression in mammalian cells

Synthetic genes for P38α/MAPK14 fused at the C terminus to human PRDX1 or PRDX2 were custom synthesized by integrated DNA technologies (IDT) and provided in the pUCIDT-Kan GoldenGate vector. Constructs were designed to include a 5′ Kozak sequence consensus sequence, an N-terminal FLAG-tag with a 3C protease cleavage site (LEVFLQG/P), a short linker region (GGGSGGG) between the two fusion proteins and a 3′ stop codon. P38α-PRDX1/2 genes were subcloned into the mammalian expression vector, pcDNA3 using BamHI and NotI (NEB) restriction enzyme and T4-ligase (NEB) following standard ligation protocols, and verified by sequencing (Eurofins). N-terminal FLAG-tagged P38α containing 3C protease site was amplified by PCR using CloneAmp HiFi PCR Premix (Takara) and ligated in to pcDNA3 using the aforementioned restrictions sites. Cysteine to serine Prdx mutants were generated using standard PCR-based mutagenic procedures.

Analysis of mammalian cellular proteins

Whole cell lysates were collected 48 h post transfection in bromophenol blue–free SDS-PAGE sample buffer supplemented with 1% (v/v) Triton X-100, protease inhibitor cocktail tablet, and a phosphatase inhibitor tablet (Roche), and sonicated briefly. Total cell lysates were clarified by centrifugation at 20,817 x *g* for 20 min at 4°C, and supernatants were sampled and diluted 30-fold to calculate protein concentration using the Coomassie Plus Staining Reagent (Bradford) Assay Kit (Thermo Fisher Scientific). Cell lysates were then normalised and processed for immunoblotting.

For immunoprecipitation experiments, proteins were harvested 48 h post transfection in a lysis buffer containing 50 mM Tris-HCl (pH 7.4), 150 mM NaCl, 0.1% (v/v) Triton X-100, 1 mM DTT, 0.1 mM ethylenediaminetetraacetic acid (EDTA), 0.1 mM ethylene glycol-bis(β-aminoethyl ether)-*N*,*N*,*N*′,*N*′-tetraacetic acid (EGTA) and 5% (v/v) glycerol and supplemented with a protease inhibitor cocktail tablet and a phosphatase inhibitor tablet (Roche). Lysates were briefly sonicated on ice and clarified by centrifuged at 20,817*g* for 20 min at 4°C, and the resulting supernatants were incubated with anti-FLAG G1 Affinity Resin (GeneScript) for 1-3 hours (as required) with gentle agitation at 4°C. Affinity beads containing bound protein were collected and washed three times in 50 mM Tris-HCl (pH 7.4) and 500 mM NaCl and then equilibrated in storage buffer (50 mM Tris-HCl [pH 7.4], 100 mM NaCl, 1 mM DTT, and 5% (v/v) glycerol). The purified proteins were then proteolytically eluted from the suspended beads over a 1-hour period using 3C protease (0.5 μg) at 4°C with gentle agitation. Purified protein was detected by western blotting using antibodies with specificity towards P38.

In vitro protein kinase assays using immunoprecipitated P38 or P38-Prdx fusion proteins

Nonradioactive kinase assays were performed using real-time mobility shift-based microfluidic assays, as described previously,[10] in the presence of 2 μM of the appropriate fluorescent-tagged peptide substrate (5-FAM-IPTSPITTTYFFFKKK-COOH), 1 mM ATP and 1 mM DTT. Pressure and voltage settings were adjusted manually to afford optimal separation of phosphorylated and nonphosphorylated peptides. All assays were performed in 50 mM Hepes (pH 7.4), 0.015% (v/v) Brij-35, and 5 mM $MgCl_2$, and real-time peptide phosphorylation was calculated from the ratio of the phosphopeptide:peptide. Where specified, assays also included 10 μM of the selective P38 inhibitor SB239063 (Tocris).

Analysis of *S. pombe* proteins by immunoblotting

For cell extracts prepared under native protein (non-denaturing) conditions: Equal numbers of approximately 2-2.5x10^8 exponentially growing *S. pombe* were mixed with an equal volume of ice pelleted by centrifugation for 1 min then snap frozen in liquid nitrogen. Cell pellets were thawed and suspended in ice cold lysis buffer (50mM Tris.Cl pH 7.5, 150mM NaCl, 0.5% (v/v) NP40) containing protease inhibitors (1μg/ml leupeptin, 1μg/ml pepstatin, 1% (v/v) aprotinin and 0.5mg/ml phenylmethylsulfonyl fluoride) and phosphatase inhibitors (50mM sodium fluoride and 2mM sodium vanadate) then transferred to 1ml ice-cold glass beads and disrupted using a Mini Beadbeater-16 (Biospec products) to obtain cell lysates, essentially as described previously.[71] Insoluble material was pelleted by centrifugation and soluble proteins present in supernatant retained for analysis.

For whole cell extracts (SDS-extracted proteins): Equal numbers of exponentially growing *S. pombe* (4.5×10^7-5×10^7) were added to 20% (w/v) trichloroacetic acid (TCA), harvested by centrifugation and snap frozen in liquid nitrogen. Pelleted cells were suspended in 10% (w/v) TCA and disrupted using ice cold glass beads and a Mini Beadbeater-16 (Biospec products) essentially as described previously.[72] Following cell lysis, TCA-precipitated proteins were acetone-washed before resuspension in 1% (w/v) SDS, 1 mM EDTA, 100 mM Tris-HCL pH 8.0. In experiments where oxidation state was examined, (e.g. Pyp1 in Figure 2 or Sty1 in Figure 3B), proteins were dissolved in TCA buffer containing 10 mM *N*-Ethylmaleimide (NEM) or, where indicated (Figure 2E), 25mM 4′-acetamido-4′-maleimidylstilbene-2,2′-disulfonic acid (AMS) to prevent disulfide exchange and visualize any shifts due to cysteine oxidation. EDTA-free TCA buffer was used where phosphorylation of proteins was to be investigated by alkaline phosphatase-treatment (Roche) or Phos-tag™ (NARD Institute, Japan) gels. Protein concentrations were estimated using the bicinchoninic acid protein assay (Thermo scientific). For phosphatase-treatment, approximately 15μg total protein was treated with 1-2μl of 20u/μl alkaline phosphatase (Roche) or 1-2μl EDTA-free TCA buffer for 1h at 37°C. Equal amounts of denatured protein were separated by SDS-PAGE on 8% acrylamide gels containing 100mM Phos-tag™ where indicated. Separated protein was then transferred onto nitrocellulose membrane (GE healthcare) or, for Phos-tag gels, methanol-activated PVDF membrane (Immobilon-P Milipore). Where indicated, membranes were staining with Revert™ 700 total protein stain (LI-COR) for normalization of protein loading. Membranes were then blocked in TBS-T (15mM NaCl, 1 mM Tris-HCl pH8.0, 0.01% Tween-20) containing 10% (w/v) bovine serum albumin (BSA) for 1 hour at room temperature before incubation overnight at 4°C with the indicated primary antibodies diluted 1 in 1000 with 5 % (w/v) BSA in TBS-T.

Size exclusion chromatography analysis of native protein extracts

Native protein extracted as described above (in 0.5% NP40, 1μg/ml leupeptin, 1μg/ml pepstatin, 1% (v/v) aprotinin, 0.5mg/ml phenylmethylsulfonyl fluoride, 50mM sodium fluoride and 2mM sodium vanadate) were separated using a Superose™6 10/300 GL column (Cytiva Life Sciences, UK) on a low pressure FPLC system pre-equilibrated with 30ml lysis buffer (50mM Tris.Cl pH 7.5, 150mM NaCl) before injection of 500μl freshly prepared cell lysate. Buffer flow rate was 0.5ml/min throughout and 0.5ml fractions were collected over 20ml. To calibrate the column, standard globular proteins (Cytiva Life sciences, UK), Bovine Serum Albumin (BSA) (66kDa), Ferritin (440kD) and Thyroglobulin (669kDa) were run under the same conditions as the extracts. Dextran Blue (2000kDa) was used to demonstrate the void volume of the column was ~7ml. Fractions were stored on ice until further processing (within 1h of elution). Proteins were denatured by addition of 6x SDS loading buffer (375mM Tris-HCL (pH 6.8), 9% (w/v) SDS, 50% glycerol, 9% (v/v) β-mercaptoethanol, 0.03% (w/v) bromophenol blue) before separation by SDS PAGE alongside 0.4% input (2μl of cell lysate) and immunoblotting. Fraction of input protein present in lane was determined from LI-COR quantification of protein signal relative to signal from input lane analyzed on the same gel.

Antibodies

Mouse monoclonal anti-Myc (9E10, Santa Cruz Biotechnology), anti-HA (HA-7, Sigma-aldrich), anti-FLAG or anti-Pk (V5 Tag) antibodies (Sigma-aldrich) were used for detecting epitope-tagged proteins. anti-phospho-P38 antibody (Thr180/Tyr182 Cell signalling) were used to detect the dual phosphorylated forms of Sty1 or P38. Total P38 and GAPDH from mammalian extracts were detected using rabbit-derived antibody from Cell Signalling. Rabbit polyclonal anti-Hog1 antibodies (Y-215, Santa Cruz Biotechnology) or anti-Sty1[39] antibodies were used to detect Sty1. Protein bands were visualised using the LI-COR Odyssey CLx system with LI-COR secondary antibody (IRDye 800 CW anti-rabbit/mouse) or anti-mouse IgG (whole molecule) (A4416) or anti-rabbit IgG (Sigma-Aldrich) conjugated to horseradish peroxidase.

Imaging and quantification of immunoblots

For Phos-tag™ gels and experiments in Figures 2E, S1, and S4; enhanced chemiluminescence (PierceTM ECL Plus, Thermo Scientific) and ImageQuant Software (Typhoon FLA9500) or X ray film (Fuji) was used to visualise detected proteins. All other immunoblots

were imaged and quantified using LI-COR Image studio Lite. For quantification of experiments using whole cell lysates prepared under native or denaturing conditions: Lane normalization factor (LNF) was calculated from total protein stain (Revert™ LI-COR) on 700 nm channel by selecting individual rectangles for appropriate, equal-sized part of each lane after background subtraction in adjacent area (top and bottom/right and left). Total protein stain at 700nm was removed using Revert destaining solution (Revert™ LI-COR) prior to blocking, if the protein of interest was to be detected using 700nm channel. The signal of protein of interest was selected from either 700nm or/and 800nm channel (dependent on secondary antibody used) with background subtraction. Target protein signals were normalised to total protein by dividing by the lane normalization factor for that lane. For quantification of the distribution of Wis1 and Sty1 in fractions obtained by size exclusion chromatography (Figure 6D), protein signals were expressed relative to the Wis1 or Sty1 signal from an 'input' lane on the same gel in which 0.4% of cell lysate was separated.

Determining *S. pombe* cell size at division

Cells that had been maintained continuously in exponential phase for 18-24 hrs were pelleted at OD_{595} 0.1. Cells were fixed in 3.7% (w/v) formaldehyde solution for 10 min at room temperature, washed twice in phosphate buffered saline (PBS) (137 mM NaCl, 2.7 mM KCl, 10 mM Na_2HPO_4 and 1.8 mM KH_2PO_4) then resuspended in 10μl PBS solution containing 0.67 mg/ml Calcofluor (Sigma). Stained cells were mounted in Vectashield containing 1.5μg/ml 4, 6-diamidino-2-phenylindole (DAPI)(Vector Laboratory) on poly-L-lysine coated microscope slides. Cell morphology using differential interface contrast (DIC), and septum staining with Calcofluor, were imaged using Zeiss Axiovert or Axioskop fluorescence microscope (excitation wavelength 359nm and emission wavelength 461nm. The length of septum-stained cells was determined using Axiovision software for at least 150 cells per group.

Analysis of S. pombe cell volume using a cell counter

40μl of exponentially growing cells (OD595 0.3-0.5) were added to 10ml of CASYton solution, and following sonication, 3 repeated measurements of ~6,000 cells were made on the CASY Cell Counter + Analyser System, ModelTT (Schärfe System).

Experiments involving cells expressing analogue-sensitive $Sty1^{T97A}$ mutants

SISA strains KS8266 and KS8311[49] were maintained on Ye5S media containing 5μM 3-BrB-PP1(Abcam, ab143756) to prevent activation of sty1 and retention of $Wis1^{DD}$ was confirmed by sequencing of cells used for experiments. For detecting Sty1 and Wis1 phosphorylation before and after oxidative stress, overnight SISA cells were grown in EMM media with supplements containing 5μM 3-BrB-PP1. Cells were diluted to OD_{595} 0.15 next day in the same media until reaching OD_{595} 0.5. Cell pellets were collected by <1 min centrifugation at < 2000rpm washed twice (one culture volume per wash) in either EMM media or EMM media containing 5 μM 3-BrB-PP1 before transfer to fresh EMM or EMM containing 5 μM 3-BrB-PP1 and treatment (where indicated) with 6 mM H_2O_2.

QUANTIFICATION AND STATISTICAL ANALYSIS

Quantification of immunoblotting and cell length measurements were carried out as described in method details above. Each immunoblotting experiment shown in figures is representative of results from at least 3 independent biological repeats. Where genetic interactions were examined, results were repeated in multiple independent isolates in comparison with isogenic strains derived from the same cross. All experiments involving cell length measurements were repeated at least twice and results from representative experiments are shown. Error bars on graphs or in tables represent the standard error of the mean. As indicated, Student's T tests were used to identify any quantitative differences between strains that were statistically significant and any differences $p<0.05$ are reported in figure legends.